

https://dspace.org/

Major trace element and SrNd isotope evidence for a sublithospheric mantle source for the Umkondo large igneous province

Ben Hayes; Lewis Ashwal; Khulekani Khumalo; Linda Iaccheri

https://hdl.handle.net/10539/41057
WOS

Downloaded from a DSpace repository. https://dspace.org/

Geoscience Frontiers 15 (2024) 101719

Contents lists available at ScienceDirect

Geoscience Frontiers

journal homepage: www.elsevier.com/locate/gsf

Research Paper

Major, trace element and Sr-Nd isotope evidence for a sublithospheric mantle source for the Umkondo large igneous province

Ben Hayes *, Lewis D. Ashwal, Khulekani B. Khumalo, Linda M. Iaccheri

School of Geosciences, University of the Witwatersrand, Johannesburg, 2050, South Africa

ARTICLE INFO

Article history:
Received 14 November 2022
Revised 10 August 2023
Accepted 30 September 2023
Available online 5 October 2023
Handling Editor: C. Manikyamba

Keywords:
Umkondo large igneous province
Low-Ti magma
Continental tholeiites
Sublithospheric mantle sources
Kalahari craton
Rodinia

ABSTRACT

The Mesoproterozoic (1.11 Ga) Umkondo large igneous province (LIP) in southern Africa and Antarctica was emplaced in < 5 Myr and is dominated by low-Ti tholeiitic doleritic-gabbroic sills. It is of particular interest because it is the least studied LIP in southern Africa with both sublithospheric and lithospheric mantle sources proposed and it coincides with the early assembly of Rodinia, so it has importance in understanding the nature of magmatism and tectonics in and around the Kalahari craton during the Mesoproterozoic. In this study, we compiled a large database of existing (~750) and new (~100) major and trace element data for the Umkondo province, as well as 42 new Sr-Nd isotopic measurements, to provide constraints on its magma sources and geochemical evolution. Major element compositional variations in the low-Ti tholeiites are explained by low-pressure (1 kbar) three-phase fractional crystallisation (olivine, clinopyroxene and plagioclase) of a parent magma with ~ 10 wt.% MgO in oxidising conditions (QFM + 1). Inverse models show that the low-Ti tholeiitic magmas were derived as residual melts after the crystallization of 12%–33% olivine from primary komatiitic-basaltic magmas (up to ~ 20 wt.% MgO) in equilibrium with mantle olivine (Fo_{90}). Low Sm/Yb and TiO_2/Yb-Nb/Yb indicate that the primary magmas were derived by 2%–20% shallow (40–50 km) partial melting of spinel lherzolite. High Sm/Yb is restricted to dyke swarms and may imply limited magma production from deeper (up to ~ 70 km) garnet lherzolite-like sources. The low-Ti tholeiites of the Umkondo province are enriched in large ion lithophile elements (Rb-Sr-Cs-K) and depleted in high-field strength elements (Zr-Hf-Nb-Ta), indicating the involvement of crustal material and/or the subcontinental lithospheric mantle. This is supported by covariations in Th/Nb, Nb/Yb, Nb/La and Ce/Sm with generally negative ΔNb. Sr-Nd isotopes lend support to the notion that the Umkondo magmas were derived from depleted and/or enriched sublithospheric mantle sources and subsequently contaminated by enriched lithospheric material during emplacement (initial (at 1.11 Ga) $^{87}Sr/^{86}Sr$ between 0.704820 and 0.737464 and εNd between −8.9 and +5.3). The Vredefort sills are significant as they display the most depleted Sr-Nd isotopic signatures (average initial $^{87}Sr/^{86}Sr$ of 0.705342 and average εNd of 0.4) and are the least contaminated magma suite in the Umkondo province. Because of (i) the large volume of low-Ti magmas, (ii) evidence of a primary hot and MgO-rich (komatiitic) magma, and (iii) the short duration of magmatism, we suggest that the Umkondo province was formed by plume-induced melting of the sublithospheric mantle beneath the Kalahari craton in an extensional setting. This contrasts with previous suggestions that the heat source developed in response to the "thermal insulation" of the mantle beneath a thickened Kalahari craton in the absence of a mantle plume. There is further evidence from the elevated Zn/Fe that the sublithospheric mantle was lithologically heterogeneous and consisted of mixed peridotite and pyroxenite domains. There is a general lack of ultramafic cumulates in the low-Ti magma suite that may imply there was deeper ponding and storage of the primary magmas that fractionated large quantities of ultramafic rocks. There is also a paucity of high-Ti rocks in the Umkondo province that may reflect limited direct melting of the lithospheric mantle or that they are simply not as well-preserved in this province compared to the Karoo province. The similar trace element and Sr-Nd isotopic compositions of the Umkondo sills in southern Africa with the Borgmassivet sills in Antarctica support the concept that the Kalahari craton and Grunehogna terrane were adjoined at 1.11 Ga. The timing of the

* Corresponding author.
E-mail address: ben.hayes@wits.ac.za (B. Hayes).

https://doi.org/10.1016/j.gsf.2023.101719
1674-9871/© 2023 China University of Geosciences (Beijing) and Peking University. Published by Elsevier B.V. on behalf of China University of Geosciences (Beijing).
This is an open access article under the CC BY-NC-ND license (http://creativecommons.org/licenses/by-nc-nd/4.0/).

Umkondo province indicates there was localised lithospheric extension and upwelling asthenospheric mantle during a time of dominantly compressional tectonics on Earth at the end of the 'boring billion'.
© 2023 China University of Geosciences (Beijing) and Peking University. Published by Elsevier B.V. on behalf of China University of Geosciences (Beijing). This is an open access article under the CC BY-NC-ND license (http://creativecommons.org/licenses/by-nc-nd/4.0/).

1. Introduction

Large Igneous Provinces (LIPs) are products of vast amounts of basalt emplaced in the crust or erupted at the Earth's surface typically in a short period of geological time (<5 Myr: Courtillot and Renne, 2003) occurring in both continental and oceanic settings (Ernst, 2014). The short duration and large volumes of LIP magmatism are typically explained by plume-induced melting of the mantle (Hart et al., 1992; White and McKenzie, 1995; Condie, 2001). The magma sources of the basalts are thought to be represented by either the sublithospheric mantle (e.g., Arndt et al., 1993; Andersen, 1994; Ashwal, 2021) or the lithospheric mantle (e.g., Gallagher and Hawkesworth, 1992; Turner et al., 1996; Jourdan et al., 2009) or a combination of both (e.g., Bédard et al., 2021). The chemical distinction between these sources is hampered by the magma interacting with continental reservoirs during emplacement.

Continental tholeiites have distinctive chemical signatures such as K-Rb-Th-U enrichment and Nb-Ta-Ti depletion that imply interaction with a continental reservoir. The origin of these chemical signatures has been explained by the derivation of tholeiitic magmas from ocean island basalt (OIB) sources and subsequent contamination by the lithospheric mantle and/or continental crust (e.g., Carlson et al., 1981; DePaolo, 1981; Wooden et al., 1993; Heinonen et al., 2016; Ashwal, 2021). An alternative hypothesis is that asthenospheric mantle-derived magmas may assimilate partial melts of enriched domains in the lithospheric mantle (Ellam and Cox, 1991; Jourdan et al., 2007; Zhang et al., 2008; Rooney et al., 2017). Another view is that recycled enriched continental material may be part of the mantle source (Tegner et al., 2019). In the investigation of the mantle sources of continental tholeiites, it is critical to assess the chemistry of various magmatic domains in a single LIP (Ernst, 2014). A better understanding of the chemical diversity and its spatial distribution aids in establishing the heterogeneity of the sources and the geochemical evolution of the magmas during mantle-crust transfer.

There is an excellent natural laboratory in southern Africa to study magma sources and the influence of lithosphere and crust in the evolution of continental flood basalt provinces. There are at least four spatially overlapping and well-preserved LIPs on the Kalahari craton that span 2.5 billion years (Ashwal, 2021). There is the Neoarchean Ventersdorp province (~2.78 Ga), the Paleoproterozoic Bushveld Complex (2.06 Ga), the Mesoproterozoic Umkondo province (1.11 Ga), and the Mesozoic Karoo province (0.18 Ga). Sublithospheric and lithospheric mantle sources have been proposed by various authors for each of these provinces (as summarised in Ashwal, 2021). The most well-studied is the young, and well-exposed Karoo province, for which the high- and low-Ti magma types were recognised (Cox et al., 1967). The most recently discovered of these four major continental basalt provinces is the Umkondo province (Hanson et al., 1998), however, it is also the least well-studied and there are few constraints on its magma sources and petrogenesis.

The Umkondo province extends across an area of $\sim 2 \times 10^6$ km^2 on the Kalahari craton and Grunehogna terrane (Antarctica) and is comparable in size and volume to the 2×10^6 to 3×10^6 km^2 Karoo province (Hanson et al., 2004). It is dominated by exposures of gabbro-dolerite sills with subordinate layered mafic–ultramafic intrusions, radial dyke swarms, and lavas. We compiled all existing geochemical data for the Umkondo province (~750 samples) and include a suite of new major and trace element data (~100), as well as 42 new Sr-Nd isotopic measurements, for the different magmatic domains in the province. We use these data to provide a detailed summary of the magma types, their sources, and the evolution of the magmas in the Umkondo province. The nature and timing of Umkondo magmatism also have implications for the early tectonics of the Rodinia supercontinent in the Mesoproterozoic near the end of the boring billion.

2. Umkondo large igneous province

The Umkondo large igneous province (LIP) is named after the exposures of thick and extensive dolerite sills in the Paleoproterozoic-aged Umkondo Group of eastern Zimbabwe. Early paleomagnetic and age-dating studies showed that the Umkondo sills, along with the Timbavati gabbros and the Vredefort sills of northeastern South Africa, were part of a single magmatic province (McElhinny and Opdyke, 1964; Jones and McElhinny, 1966; Allsopp et al., 1989). High-precision ages of these dolerite sills across the entire Kalahari craton led to the classification of the Umkondo province as a single LIP that was emplaced at ca. 1.11 Ga over a duration of < 5 Myr (Hanson et al., 2004). There are mafic dyke swarms and contemporaneous volcanic basalt-rhyolite magmatism that may also be part of the Umkondo province (Hanson et al., 2006). Sills and lavas of the Umkondo age are also recognised on the Grunehogna terrane in Antarctica (Moyes et al., 1995; Hanson et al., 2004; Riley and Millar, 2014). The spatial distribution of the Umkondo province, and its magmatic domains, is shown on a reconstructed Kalahari craton in Fig. 1.

3. Domains of Umkondo magmatism and existing geochemical data

The Umkondo province consists mostly of gabbro-dolerite sills that are widespread across southern Africa (Fig. 1) and which were emplaced into fault-bound Paleoproterozoic supracrustal sequences and Archean granite-gneisses. Dolerite sill complexes emplaced into clastic-carbonate sedimentary sequences include the Chimanimani sills of eastern Zimbabwe, the Waterberg sills, the Soutpansberg sills, and the Middelburg sills of northeastern South Africa, the Palapye sills of eastern Botswana, and the Borgmassivet sills of Antarctica. Dolerite sills emplaced into Archean granites include the Nyanga sills in eastern Zimbabwe and the Vredefort and Timbavati sills in northeastern South Africa. The Xade Complex is a large subsurface layered mafic–ultramafic intrusion in central Botswana. There are subordinate volcanic rocks throughout the Umkondo province. Basaltic lava remnants are preserved in the Lower Sabi Valley of eastern Zimbabwe, Espungabera in western Mozambique, and Straumsnutane in Antarctica. Some of the Umkondo sills, lavas and dykes are located near the margins of the Kalahari craton (Fig. 1). Radiating dolerite dyke swarms, including the Mutare and Guruve dykes, are distributed across the Kalahari craton and are tentatively correlated to the Umkondo province (Fig. 1; de Kock et al., 2014). We give an overview of the geology and petrology of the magmatic domains in the Umkondo

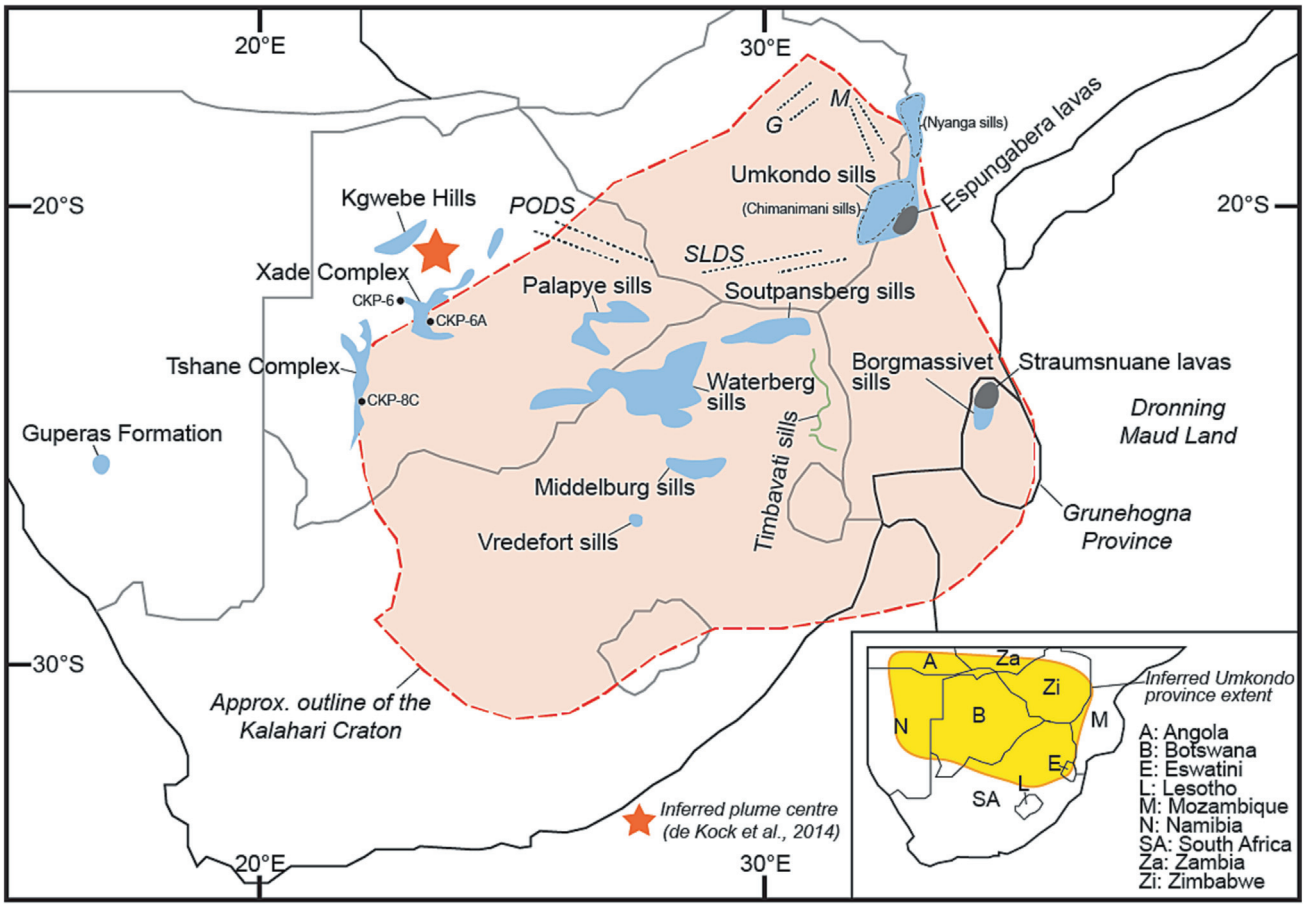


Fig. 1. A map showing the distribution of the Umkondo province (sills, lavas and dyke swarms) across southern Africa (adapted from Hanson et al., 2004). The Umkondo sills of eastern Zimbabwe are subdivided into the Chimanimani sills (in the south) and the Nyanga sills (in the north). The Kaapvaal and Zimbabwe cratons and the Grunehogna terrane are adjoined as the Kalahari craton. The inferred magmatic centre (red star) is from de Kock et al. (2014). The inset shows the distribution of the Umkondo province across southern Africa, which now extends into southern Angola (Salminen et al., 2018). CKP-6, CKP-6A and CKP-8C are drill hole locations in the Xade and Tshane Complexes of central Botswana. PODS = Proterozoic Okavango Dyke Swarm; SLDS = Save-Limpopo Dyke Swarm; G = Guruve dykes; M = Mutare dykes. (For interpretation of the references to colour in this figure legend, the reader is referred to the web version of this article.)

province, as well as a summary of the existing geochemical data, in the following subsections.

3.1. Chimanimani and Nyanga sills

The Chimanimani and Nyanga sills are collectively known as the Umkondo sills (from which the entire province takes its name), and they crop out discontinuously in eastern Zimbabwe (Fig. 1). The Chimanimani sills were emplaced into a Paleoproterozoic sequence of clastic and carbonate sedimentary rocks of the Umkondo Supergroup that unconformably overlies Archean granite-gneiss of the Zimbabwe craton. There are thick (600–1200 m) doleritic-gabbroic sills in the calcareous and argillaceous units and thinner (150–300 m) sills in the quartzitic sedimentary rocks (Watson, 1969). The mineralogy of the Chimanimani sills consists of labradorite plagioclase (molar An_{45-65}), augite, pigeonite, inverted pigeonite, olivine, minor quartz, granophyre, biotite, ilmenite, and magnetite, and which is overprinted by greenschist facies metamorphism (Ward, 2002). The lack of chilled margins and the evidence for localised brecciated contact zones has led to the suggestion that the Chimanimani sills intruded semi-lithified sediments (Munyanyiwa, 1999, and references therein). The Nyanga sills of eastern Zimbabwe were emplaced into Archean granite-gneisses. The Nyanga sills are up to 450 m thick and have very similar mineralogy to the Chimanimani sills (Ward, 2002). There are ~ 50 major and trace element analyses reported for the Chimanimani sills and 7 for the Nyanga sills (Munyanyiwa, 1999; Ward, 2002). There are ~ 46 strontium isotope data reported for the Chimanimani and Nyanga sills (including the lavas in the Lower Sabi Valley: Allsopp et al., 1989). We include 25 new major and trace element data for the Chimanimani sills and 16 for the Nyanga sills. We also include 7 new Sr-Nd isotope measurements for these sills – 4 for Chimanimani and 3 for Nyanga (Tables 1 and 2).

3.2. Waterberg sills

The Waterberg sills range in thickness between 0.3 and 120 m and were emplaced into the Paleoproterozoic Waterberg sedimentary basin in northeastern South Africa (Fig. 1). The Waterberg sills are medium-grained and have sub-ophitic textures (locally variolitic and glomeroporphyritic) that consist of labradorite plagioclase, augite, and variable amounts of olivine, magnetite, pigeonite, enstatite, biotite, and granophyre (Bullen et al., 2012). The Waterberg sills also include the 72 m thick Bellevue sill that intruded into the layered sequence of the Bushveld Complex (Ashwal et al., 2005). A similar suite of poorly-dated doleritic-gabbroic sills was emplaced into the Soutpansberg sedimentary basin and may be directly correlated with the Waterberg sills (Fig. 1). There are 63 major and trace element data (with limited hafnium and rare earth element concentrations) reported for the Waterberg sills and 5 Sr-Nd isotope measurements (Bullen et al., 2012). We include 20 new major and trace element anal-

Table 1
All new Rb-Sr isotopic measurements for 42 samples from the Umkondo province. 2 SE = 2 × standard error. The initial $^{87}Sr/^{86}Sr$ ratio was recalculated to 1.11 Ga using decay constants of 1.4×10^{-11}/year (^{87}Rb).

Sample ID	Domain	Rb (ppm)	Sr (ppm)	$^{87}Rb/^{86}Sr$	$^{87}Sr/^{86}Sr$	2 SE	Initial $^{87}Sr/^{86}Sr$ (1.11 Ga)
DB01.3	Waterberg sills	43.2	121.1	1.032	0.726033	± 0.000006	0.709645
DB01.4	Waterberg sills	57.5	145.8	1.144	0.728113	± 0.000020	0.709962
DB01.47	Waterberg sills	61.2	136.5	1.300	0.733540	± 0.000026	0.712912
DB01.52	Waterberg sills	41.7	219.4	0.552	0.746224	± 0.000006	0.737464
DB01.53	Waterberg sills	58.1	132.6	1.271	0.730309	± 0.000022	0.710141
DB01.62	Waterberg sills	11.7	166.4	0.204	0.710022	± 0.000018	0.706790
DB01.88	Waterberg sills	20.8	106.3	0.567	0.716556	± 0.000010	0.707554
DB01.89	Waterberg sills	30.6	130.8	0.677	0.719632	± 0.000006	0.708881
BV01	Bellevue sill	17.0	175.6	0.280	0.714184	± 0.000028	0.709736
BV23	Bellevue sill	49.9	196.7	0.735	0.725436	± 0.000018	0.713774
DB02.151	Vredefort sills	30.0	166.1	0.522	0.714030	± 0.000006	0.705737
DB02.152	Vredefort sills	32.9	152.3	0.625	0.715513	± 0.000006	0.705591
DB02.153	Vredefort sills	38.9	158.3	0.712	0.717090	± 0.000020	0.705786
DB02.154	Vredefort sills	23.7	156.9	0.437	0.712178	± 0.000008	0.705247
DB02.155	Vredefort sills	25.9	156.3	0.479	0.713050	± 0.000008	0.705450
DB02.156	Vredefort sills	24.1	161.0	0.433	0.712000	± 0.000008	0.705134
DB02.157	Vredefort sills	18.8	175.7	0.310	0.709890	± 0.000006	0.704968
DB02.158	Vredefort sills	18.3	154.1	0.344	0.710278	± 0.000006	0.704820
DB02.159	Vredefort sills	19.5	169.8	0.332	0.711125	± 0.000006	0.705853
DB02.160	Vredefort sills	32.5	164.2	0.572	0.714108	± 0.000014	0.705027
DB02.162	Vredefort sills	21.7	150.2	0.419	0.711806	± 0.000008	0.705154
DB02.8	Timbavati sills	10.5	79.1	0.385	0.712635	± 0.000006	0.706523
DB02.56	Timbavati sills	36.1	202.5	0.516	0.717709	± 0.000010	0.709519
DB02.60	Timbavati sills	23.9	203.9	0.339	0.712989	± 0.000014	0.707600
DB02.69	Timbavati sills	25.6	115.0	0.645	0.718087	± 0.000010	0.707846
DB02.74	Timbavati sills	26.6	124.5	0.618	0.717197	± 0.000006	0.707386
JP-1	Palapye sills	35.3	304.8	0.335	0.713143	± 0.000006	0.707826
JP-15	Palapye sills	26.1	206.9	0.365	0.718598	± 0.000006	0.712805
JP-18	Palapye sills	51.2	138.8	1.068	0.731461	± 0.000004	0.714505
JP-26	Palapye sills	36.3	128.9	0.817	0.723793	± 0.000006	0.710825
JP-33	Palapye sills	44.7	129.3	1.000	0.726902	± 0.000006	0.711030
JP-35	Palapye sills	34.6	124.4	0.807	0.723520	± 0.000006	0.710719
UMK2	Umkondo sills (Chimanimani)	57.3	138.0	1.204	0.729992	± 0.000006	0.710876
UMK7	Umkondo sills (Chimanimani)	52.4	138.0	1.100	0.727119	± 0.000006	0.709666
UMK16	Umkondo sills (Chimanimani)	81.4	153.7	1.535	0.734818	± 0.000008	0.710459
UMK22	Umkondo sills (Chimanimani)	68.5	125.4	1.584	0.734279	± 0.000008	0.709141
UMK26	Umkondo sills (Nyanga)	32.3	154.1	0.608	0.720204	± 0.000006	0.710559
UMK28	Umkondo sills (Nyanga)	49.2	132.4	1.076	0.729404	± 0.000004	0.712324
UMK31	Umkondo sills (Nyanga)	23.6	153.0	0.446	0.716897	± 0.000006	0.709824
CKP8C1-4	Xade Complex	13.53	214.40	0.183	0.709406	± 0.000006	0.706509
KD01	Guperas Formation	124.4	349.9	1.030	0.724313	± 0.000006	0.707968
KG28	Guperas Formation	59.2	394.8	0.434	0.714638	± 0.000006	0.707750

yses of the Bellevue sill and 4 new trace element analyses for the Waterberg sills. We also include 8 new Sr-Nd isotopic measurements for Waterberg sills – and 2 for the Bellevue sill (Tables 1 and 2).

3.3. Palapye sills

The doleritic-gabbroic Palapye sills of southeastern Botswana were emplaced into the supracrustal sequence of the Palapye Group and the underlying Archean-Paleoproterozoic basement rocks of the Limpopo Belt (Fig. 1; Pancake, 2001; Hanson et al., 2006; Swanson-Hysell et al., 2015). Some of the Palapye sills are relatively felsic in composition with granophyric segregations and some grade into clinopyroxene-rich granites (Hanson et al., 2006). The Palapye sills may be a western extension of the Waterberg-Soutpansberg sills (Bullen et al., 2012). There are 8 major and trace element analyses reported for the Palapye sills (Bullen, 2005). We include 6 new major and trace element analyses and 6 new Sr-Nd isotopic measurements for the Palapye sills (Tables 1 and 2).

3.4. Middelburg sills

The doleritic-gabbroic Middelburg sills are located to the southeast of the Waterberg sills (Fig. 1) and have been described from drillcore intersections, but there are few age constraints (Bullen, 2005). 37 major and trace element analyses were reported for the Middelburg sills (Bullen, 2005).

3.5. Timbavati sills

The doleritic-gabbroic Timbavati sills were emplaced into Archean basement granite-gneisses and are exposed in northeastern South Africa (Fig. 1). The Timbavati sills are laterally extensive (although discontinuous) for ~ 200 km and range in thickness between 200 and 480 m (Hargraves, 1994; Bullen, 2005; Hanson et al., 2006). The sills are medium to coarse-grained, may exhibit olivine and orthopyroxene-rich layers, and may be composite intrusions (Bullen, 2005). There are ~ 95 major and trace element analyses reported for the Timbavati sills and only 2 of these have been analysed for Sr-Nd isotopes (Bullen, 2005). Sr isotopes were reported for 6 Timbavati sills in Bristow et al. (1982). We include

Table 2
All new Sm-Nd isotopic measurements for 42 samples from the Umkondo province. 2 SE = 2 × standard error. The initial $^{143}Nd/^{144}Nd$ values ratios were recalculated to 1.11 Ga using decay constants of 6.54 × 10^{-12}/year (^{147}Sm).

Sample ID	Domain	Sm (ppm)	Nd (ppm)	$^{147}Sm/^{144}Nd$	$^{143}Nd/^{144}Nd$	2 SE	εNd (T) (1.11 Ga)
DB01.3	Waterberg sills	3.0	13.0	0.137	0.512037	± 0.000006	−3.3
DB01.4	Waterberg sills	4.1	18.3	0.135	0.512025	± 0.000012	−3.1
DB01.47	Waterberg sills	4.0	18.2	0.134	0.511939	± 0.000016	−4.8
DB01.52	Waterberg sills	4.1	18.9	0.130	0.512317	± 0.000008	3.2
DB01.53	Waterberg sills	3.9	17.8	0.134	0.511976	± 0.000012	−4.0
DB01.62	Waterberg sills	2.0	8.6	0.142	0.512050	± 0.000018	−3.7
DB01.88	Waterberg sills	2.3	9.8	0.143	0.512090	± 0.000006	−3.0
DB01.89	Waterberg sills	2.2	9.3	0.140	0.512076	± 0.000014	−2.9
BV01	Bellevue sill	3.0	12.2	0.146	0.511862	± 0.000020	−8.0
BV23	Bellevue sill	4.1	17.0	0.144	0.511797	± 0.000020	−8.9
DB02.151	Vredefort sills	4.8	19.2	0.151	0.512306	± 0.000010	0.1
DB02.152	Vredefort sills	5.0	20.0	0.152	0.512272	± 0.000006	−0.7
DB02.153	Vredefort sills	5.1	21.0	0.147	0.512537	± 0.000024	1.5
DB02.154	Vredefort sills	4.0	16.0	0.152	0.512263	± 0.000006	−1.0
DB02.155	Vredefort sills	4.1	16.6	0.150	0.512246	± 0.000006	−1.1
DB02.156	Vredefort sills	3.9	16.0	0.151	0.512303	± 0.000006	0
DB02.157	Vredefort sills	3.4	13.0	0.156	0.512343	± 0.000006	0
DB02.158	Vredefort sills	3.2	12.5	0.153	0.512245	± 0.000008	−1.5
DB02.159	Vredefort sills	3.4	13.5	0.152	0.512240	± 0.000012	−1.5
DB02.160	Vredefort sills	4.9	19.7	0.151	0.512275	± 0.000010	−0.5
DB02.162	Vredefort sills	3.4	13.8	0.151	0.512784	± 0.000012	9.3
DB02.8	Timbavati sills	1.6	7.1	0.138	0.512035	± 0.000008	−3.4
DB02.56	Timbavati sills	2.1	9.0	0.137	0.512479	± 0.000010	−3.1
DB02.60	Timbavati sills	2.7	11.6	0.141	0.512040	± 0.000012	−3.8
DB02.69	Timbavati sills	2.3	9.8	0.140	0.512076	± 0.000006	−3.0
DB02.74	Timbavati sills	2.4	10.3	0.141	0.512093	± 0.000010	−2.8
JP-1	Palapye sills	5.8	23.5	0.148	0.512100	± 0.000008	−3.6
JP-15	Palapye sills	2.8	11.5	0.147	0.511863	± 0.000010	−8.1
JP-18	Palapye sills	3.4	14.8	0.138	0.511894	± 0.000008	−6.2
JP-26	Palapye sills	2.8	12.3	0.137	0.511845	± 0.000010	−7.0
JP-33	Palapye sills	3.2	14.2	0.136	0.511835	± 0.000006	−7.1
JP-35	Palapye sills	2.8	12.3	0.137	0.511845	± 0.000008	−7.0
UMK2	Umkondo sills (Chimanimani)	3.8	16.7	0.136	0.511845	± 0.000008	−6.9
UMK7	Umkondo sills (Chimanimani)	3.3	15.1	0.132	0.511783	± 0.000006	−7.5
UMK16	Umkondo sills (Chimanimani)	4.0	18.5	0.131	0.511933	± 0.000006	−4.4
UMK22	Umkondo sills (Chimanimani)	3.6	16.3	0.132	0.511793	± 0.000006	−7.4
UMK26	Umkondo sills (Nyanga)	5.2	21.2	0.148	0.511960	± 0.000006	−6.3
UMK28	Umkondo sills (Nyanga)	3.6	16.7	0.132	0.511785	± 0.000006	−7.4
UMK31	Umkondo sills (Nyanga)	4.0	15.9	0.152	0.511980	± 0.000008	−6.4
CKP8C1-4	Xade Complex	2.6	10.2	0.152	0.512243	± 0.000006	−1.4
KD01	Guperas Formation	5.5	25.9	0.129	0.511237	± 0.000006	0.4
KG28	Guperas Formation	7.7	37.9	0.123	0.512019	± 0.000006	−1.6

9 new major and trace element analyses and 5 new Sr-Nd isotopic measurements for the Timbavati sills (Tables 1 and 2).

3.6. Vredefort sills

The doleritic-gabbroic Vredefort sills (including the Anna's Rust and Barnardskop sills) were emplaced into Archean basement granite-gneisses and metasedimentary rocks of the Witwatersrand Supergroup and are exposed in northeastern South Africa (Fig. 1). The Vredefort sills are generally fine to medium-grained, are locally plagioclase glomeroporphyritic, and some chilled margins are preserved (Reimold et al., 2000; Bullen, 2005). 12 major and trace element analyses were reported for the Vredefort sills (Bullen, 2005). We include 6 new trace element analyses and 11 new Sr-Nd isotopic measurements for the Vredefort sills (Tables 1 and 2).

3.7. Xade Complex

The Xade Complex (and Tshane Complex) is a layered mafic–ultramafic intrusion in central Botswana with an estimated thickness of 200–1000 m (Fig. 1). It is entirely subsurface and has been divided into northern and southern lobes with a total area of 45,000 km^2 (Corner et al., 2012). There are currently no published major and trace element analyses for the Xade Complex. We include 2 new major and trace element analyses and 1 new Sr-Nd isotopic measurement for the Xade Complex (Tables 1 and 2).

3.8. Borgmassivet sills

The doleritic-gabbroic Borgmassivet sills were emplaced into sedimentary rocks of the Richtersflya Supergroup, and they crop out on the Grunehogna terrane in Antarctica (Fig. 1). The Borgmassivet sills are up to 400 m thick, and, because of the similarities between the Richtersflya Supergroup and Umkondo Group, as well as similar paleomagnetic poles, they may be direct equivalents of the Chimanimani sills in eastern Zimbabwe (Groenewald et al., 1995; Jones et al., 2003; Gose et al., 2006; Riley and Millar, 2014). There are 25 major and trace element analyses reported for the Borgmassivet sills and 10 of these samples have Sr-Nd isotope data (Riley and Millar, 2014).

3.9. Umkondo lavas

There are subordinate exposures of lava in the Umkondo province. There are poorly preserved lavas in the Lower Sabi Valley,

to the west of the Chimanimani sills in eastern Zimbabwe. The lavas are described as fine-grained and porphyritic with phenocrysts of plagioclase and augite (and rare olivine) hosted in a devitrified brown groundmass (Allsopp et al., 1989). The most extensive lava sequences are the Espungabera lavas in western Mozambique and the Straumsnutane lavas in Antarctica (Fig. 1). The Espungabera and Straumsnutane lavas are fine-grained and contain plagioclase, clinopyroxene, amphibole, and Fe-Ti oxides and were affected by greenschist metamorphism (Moabi et al., 2017). 28 major and trace element analyses were reported for the Espungabera lavas and 29 for the Straumsnutane lavas (Moabi et al., 2015). Sr-Nd isotopes have been reported for 8 samples of the Espungabera and Straumsnutane lavas (Moabi et al., 2015, 2017).

3.10. Umkondo dyke swarms

Swarms of radiating dykes are distributed across southern Africa and include the Guruve, Kamativi, and Mutare dykes in Zimbabwe (Fig. 1). Some swarms have been linked to the Umkondo province based on field relations, precise age dates, and paleomagnetic data (Wilson et al., 1987; Ward, 2002; de Kock et al., 2014). The Save-Limpopo Dyke Swarm (SLDS) and Proterozoic Okavango Dyke Swarm (PODS) are also linked to the Umkondo province (Fig. 1; Jourdan et al., 2007, 2009). The Epembe-Huila dykes in southern Angola also have dates comparable to the Umkondo province (Ernst et al., 2013; Salminen et al., 2018). There are also dyke swarms in western Amazonia and in the Bundelkhand craton of India that may also be related to the Umkondo province (Choudhary et al., 2019). There are > 200 major and trace element analyses reported for the Umkondo dykes, out of which 60 have been analysed for Sr-Nd isotopes (Ward, 2002; Choudhary et al., 2019).

4. Analytical methods

We determined new bulk rock major and trace element data for 88 samples of the Umkondo province. The samples were prepared and analysed in the Earth Laboratory at the University of the Witwatersrand. Major element oxides were measured using a Panalytical PW2404 X-ray fluorescence (XRF) spectrometer. Trace element concentrations were determined by inductively coupled plasma mass spectrometry (ICP-MS) using a Perkin Elmer Elan instrument. The analytical methods and major and trace element uncertainties are described in Bourdeau et al. (2022). The complete new major and trace element data for our samples are in Supplementary Data 1.

Forty-two samples of the Umkondo province were prepared for bulk rock Sr-Nd isotopic measurements at the Wits Isotope Geosciences Laboratory (WIGL) at the University of the Witwatersrand. Approximately 300 mg of powdered sample was spiked with a mixed ^{85}Rb-^{84}Sr and ^{149}Sm-^{150}Nd tracer and then dissolved in a mixture of HF-HNO_3. Rb, Sr, Sm, and Nd were separated from the matrix by ion exchange chemistry using PFA columns (details about this method are provided in Supplementary Data 2). All isotopic measurements were determined in low-resolution mode on a Nu Instruments Plasma II MC-ICP-MS (Nu Instrument, Wrexham) housed at Spectrum (University of Johannesburg). Backgrounds were measured by offsetting the magnet away from the measuring position for 30 s prior to analyses and the signal was subtracted from the measurements. Automatic peak centering was also performed prior to each measurement. Nd measurements were collected for 60 cycles (~10 min) and Sm for 20 cycles (~5 min), achieving an internal precision of $\leq$ ± 0.001% (1 standard error) on fractionation-corrected ^{143}Nd/^{144}Nd ratios. Sr analyses were collected for 60 cycles and Rb for 20 cycles, achieving an internal precision of $\leq$ ± 0.001% (1 standard error) on fractionation-corrected ^{87}Sr/^{86}Sr ratios. Washout between samples (both Sm-Nd and Rb-Sr) was carried out using a 2% HNO_3 solution to decrease the signal-to-background values (~5 min).

Overall, all the analysis sessions, certified reference materials (BCR2, BHVO2, and AGV2) and reference materials (NIST-SRM987 and JNdi) were measured to ensure quality and reproducibility. The full Rb-Sr and Sm-Nd isotope results for the Umkondo province are included in Tables 1 and 2, respectively, as well as the online Supplementary Data 2. This appendix also contains the results of the certified reference materials.

5. Results

This section contains descriptions of the existing and new major, trace element and Sr-Nd isotope data for the Umkondo province.

5.1. Major elements

The Umkondo sills are generally classified as sub-alkaline basalts to basaltic-andesites (Fig. 2). The more evolved compositions (andesite-dacite-rhyolite) in the Umkondo sills are evolved silicic segregations present in some of the more differentiated sills and are partly alkaline. The Umkondo dykes and lavas have similar compositions to the sills. The coeval bimodal volcanic rocks range from alkaline basalts to sub-alkaline rhyolites (Fig. 2).

On major element oxide variation diagrams (Fig. 3), the Umkondo province samples show increasing SiO_2 content with decreasing MgO content (Fig. 3a) and inflexion in CaO and Al_2O_3 contents at ~ 7.5 wt.% MgO (Fig. 3c, e). This can be explained by the addition of plagioclase and clinopyroxene on the liquidus after olivine-only crystallisation at MgO contents > 7.5 wt.% (e.g., Cox, 1980). The inflexion in TiO_2 and Fe_2O_3 contents at ~ 5 wt.% MgO marks the onset of Fe-Ti oxide crystallisation (Fig. 3b, d). Na_2O shows similar patterns to CaO although the Umkondo lavas and bimodal units show elevated Na_2O contents compared to the majority of the Umkondo data (Fig. 3f). The presence of magnetite in the Umkondo sills can be explained by the magmas being relatively oxidised (Ward, 2002). There is enrichment in MgO (up to 30 wt.%) in some of the Umkondo sills, particularly in the Timbavati sills, that can be explained by olivine accumulation. The projected composition of the olivine which accumulated in the Timbavati sills is Fo_{86-87} as determined by least-squares regression.

5.2. Trace elements

On MgO-trace element concentration variation diagrams, some of the Umkondo sills show strong positive correlations in Ni and Cr that are consistent with olivine (±orthopyroxene) accumulation in the Timbavati sills (Fig. 4a, b). The Timbavati sills also have some of the lowest Zr and Sr concentrations (50–100 ppm) that are consistent with their cumulate nature (Fig. 4d, e). One of the Xade Complex samples appears to be concentrated in Fe-Ti oxides because of its enrichment in V (Fig. 4c). The Umkondo dykes and lavas generally show similar trends to the sills, but with more Sr-enriched samples in the dykes (Fig. 4e, f) that may be caused by the accumulation of plagioclase phenocrysts or the presence of Sr-enriched glass (e.g., Ashwal et al., 2021).

5.2.1. Ce/Yb-TiO_2

The low-Ti Umkondo province generally has high Ce/Yb (Fig. 5a) compared to the low-Ti suite of the Karoo province (Fig. 5b). The Umkondo dykes, and some of the Umkondo sills (e.g., Chimanimani

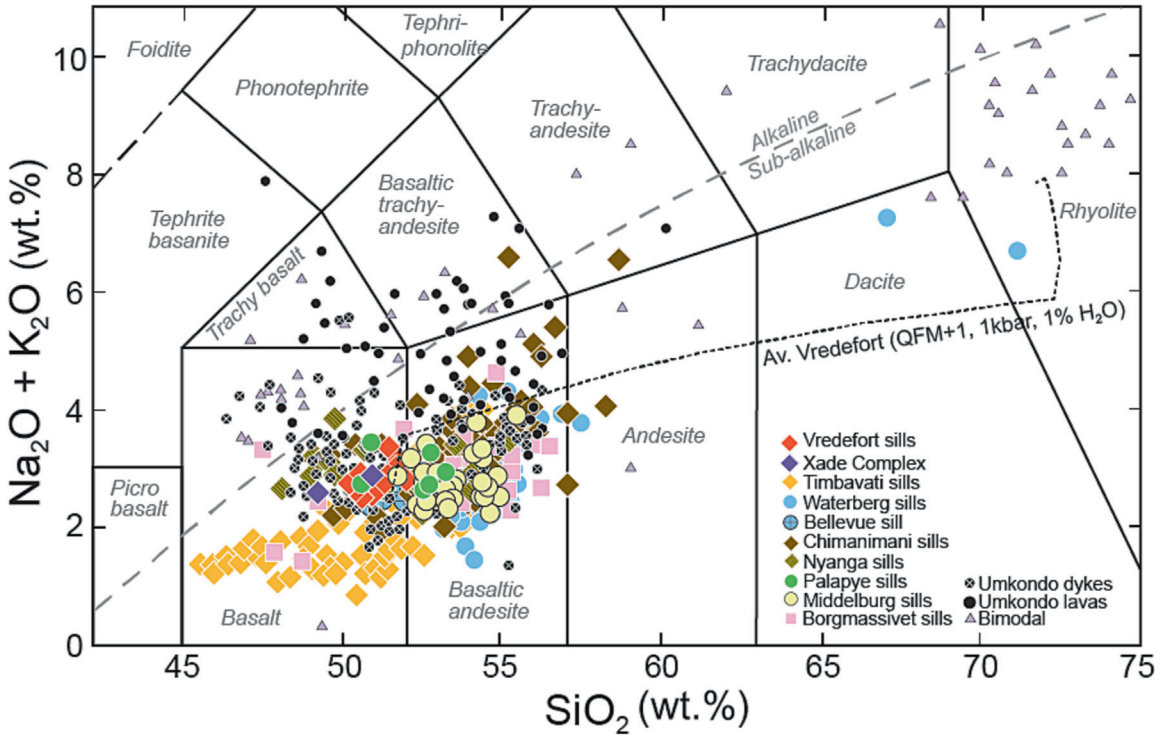


Fig. 2. A total alkali ($Na_2O + K_2O$) versus SiO_2 diagram for the Umkondo large igneous province (Le Maitre, 1984). The dashed line shows the compositional evolution of a Vredefort sill (DB02.162) according to rhyolite-MELTS (at QFM + 1, 1 kbar pressure and containing 1 wt.% H_2O).

and Nyanga), have some of the highest Ce/Yb in the province. The Chimanimani and Nyanga sills have low TiO_2 contents (<1 wt.%), whereas the dykes with a high Ce/Yb have the highest TiO_2 contents (>2–3.5 wt.%). The Vredefort sills and Xade Complex have some of the lowest Ce/Yb in the province (Fig. 5a). Some of the Timbavati and Borgmassivet sills also have low Ce/Yb. The Umkondo lavas have Ce/Yb comparable to the Umkondo sills, although at greater concentrations of Yb (Fig. 5a).

In general, the Umkondo province is characterised by low-Ti rocks compared to the Karoo province, which is subdivided into low-Ti and high-Ti suites, albeit the high-Ti suite is a minor component of the Karoo province (Ashwal, 2021) and which has some of the highest Ce/Yb. There are Umkondo dykes with greater TiO_2 contents (>2–2.5 wt.%) along with a few sills (Fig. 5b). The Vredefort sills and Xade Complex have TiO_2 contents that are intermediate to the majority of the Umkondo sills and dykes (Fig. 5b).

5.2.2. Rare earth elements

Chondrite-normalised rare earth element (REE) diagrams show the light/heavy rare earth element enrichment of the Umkondo province (Fig. 6). The sills, dykes, and lavas have comparable slopes and are typically 10 × to 100 × enriched relative to the REE concentrations of chondrites. Slight negative Eu anomalies are common and are most prominent in the Waterberg, Chimanimani, and Borgmassivet sills, and the Espungabera and Straumsnutane lavas (Fig. 6). The Vredefort sills (and Xade Complex) have some of the flattest slopes and are some of the least enriched in REE (Fig. 6). The Timbavati sills are some of the least enriched in total REE content in the entire Umkondo province. The Umkondo dykes show the widest range in terms of REE concentration (Fig. 6).

5.2.3. Multiple-element diagrams

The entire Umkondo province shows similar patterns in multiple-element diagrams (normalised to primitive mantle) with negative Nb-Ta-Th-U-Sr and positive Ti-K-Ba-Rb-Pb (Fig. 7). Negative Eu signatures are present in some of the Umkondo sills and dykes and are particularly prevalent in the Straumsnutane lavas. The Umkondo dykes show greater variability in their incompatible trace element concentrations with both positive and negative Ti, positive Rb-Ba, and negative Th-U. It was shown by Ward (2002) that the Guruve, Kamativi and Mutare dykes have very similar patterns to the Umkondo sills of eastern Zimbabwe.

5.3. Radiogenic Sr-Nd isotopes

We have collected 42 new Sr-Nd isotopic measurements for samples across the entire Umkondo province (Tables 1 and 2). This is in addition to the existing 52 combined Sr-Nd isotope data that have been published for the Umkondo province (sources listed in Fig. 8 caption). All these Sr-Nd data are plotted in Fig. 8a at their initial values (i.e., age-corrected to 1.11 Ga). There are a further 88 Sr-only isotope data for the Umkondo sills of eastern Zimbabwe (including the dykes and lavas) that show similar initial $^{87}Sr/^{86}Sr$ compositions to the data shown in Fig. 8a, although we do not include these data here, as they lack Nd isotopes.

The Palapye sills (initial $^{87}Sr/^{86}Sr$ between 0.707826 and 0.714505 and εNd between −3.6 and −8.1), Umkondo sills (initial $^{87}Sr/^{86}Sr$ between 0.709141 and 0.712324 and εNd between −4.4 and −7.5) and Waterberg sills (initial $^{87}Sr/^{86}Sr$ between 0.706790 and 0.737464 and εNd between 3.2 and −8.9) show the most enriched isotopic signatures and are comparable to the previously Sr-Nd data published for some of these sills (Fig. 8a). The two Bellevue samples (BV1 and BV23) are the most isotopically enriched samples amongst the Waterberg sills (Fig. 8a). The Timbavati sills (initial $^{87}Sr/^{86}Sr$ between 0.706523 and 0.709519 and εNd between 5.3 and −3.8), along with some of the Waterberg sills, show some of the least enriched isotopic signatures and are comparable to the previously published isotopic data for the Timbavati sills and Borgmassivet sills (Fig. 8a). The Vredefort sills (initial $^{87}Sr/^{86}Sr$

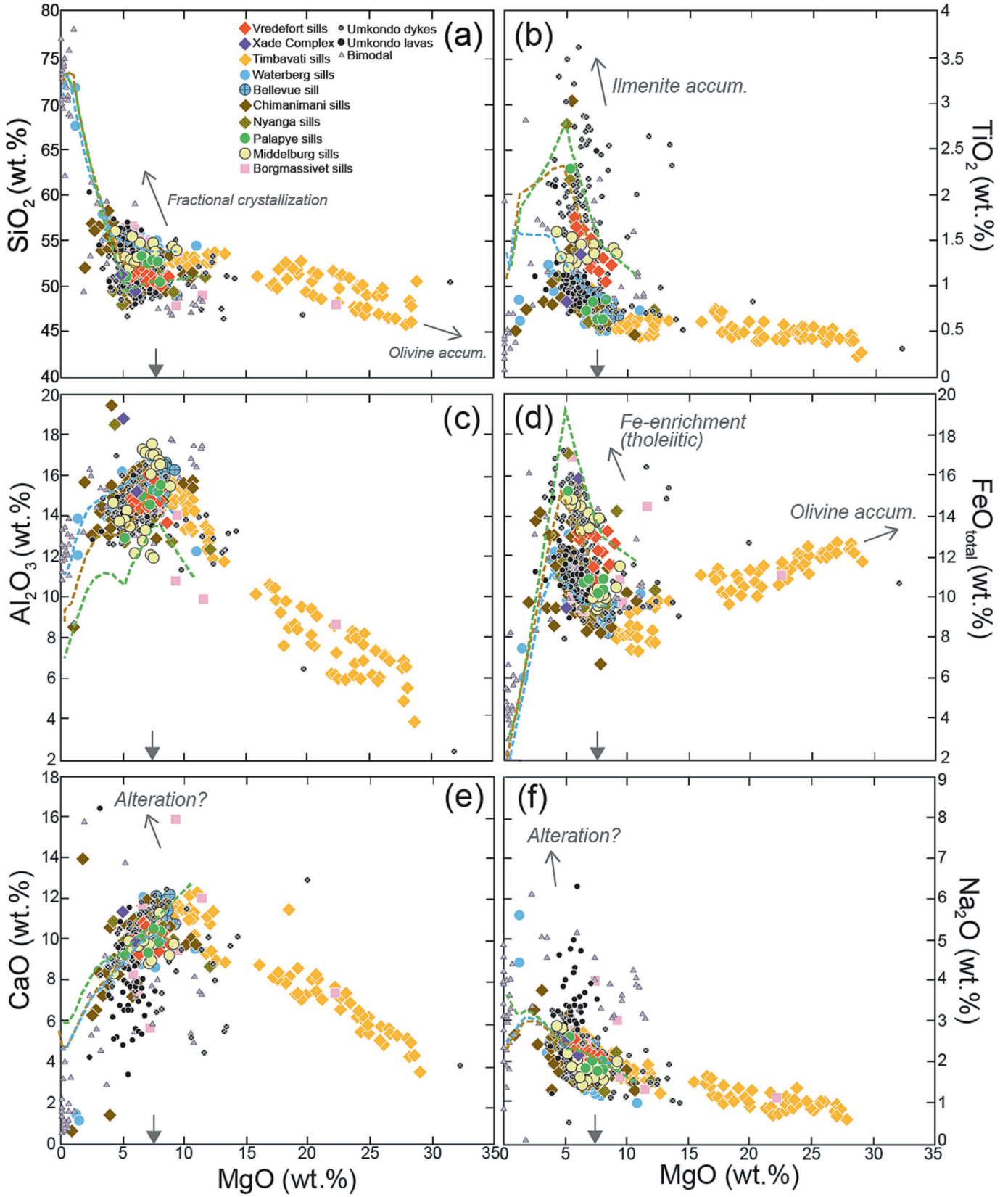


Fig. 3. Major element variation diagrams showing MgO versus SiO_2 (a), TiO_2 (b), Al_2O_3 (c), FeO (total iron) (d), CaO (e), and Na_2O (f). The coloured lines show the compositional evolution of selected Umkondo magma types according to rhyolite-MELTS (green = Z.1815.1; brown = DB02.162; blue = UMK24 at QFM + 1, 1 kbar pressure and containing 1 wt.% H_2O). (For interpretation of the references to colour in this figure legend, the reader is referred to the web version of this article.)

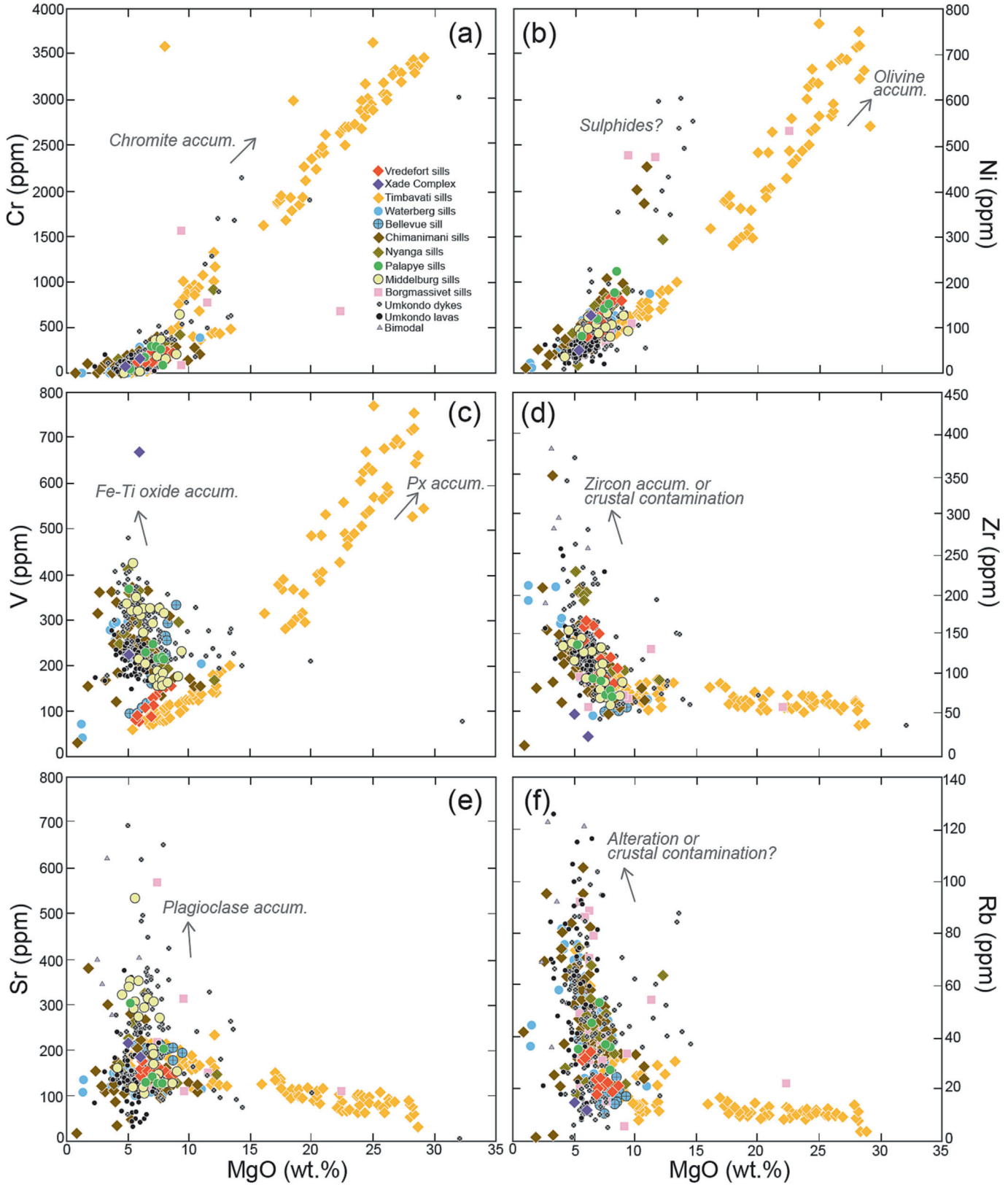


Fig. 4. Trace element variation diagrams showing MgO versus Cr (a), Ni (b), V (c), Zr (d), Sr (e), and Rb (f).

between 0.704820 and 0.705853 and εNd between 1.5 and −1.5) and Xade Complex (initial $^{87}Sr/^{86}Sr$ of 0.706509 and εNd of −1.4) show the least enriched Sr-Nd isotopic compositions and are between depleted mantle and enriched mantle endmembers (Fig. 8a). The 2 samples from the Guperas Formation (initial $^{87}Sr/^{86}Sr$ between 0.707968 and 0.707750 and εNd between 0.4 and −1.6) have similar Nd isotopic compositions to the Vredefort sills, but with more radiogenic Sr compositions (Fig. 8a).

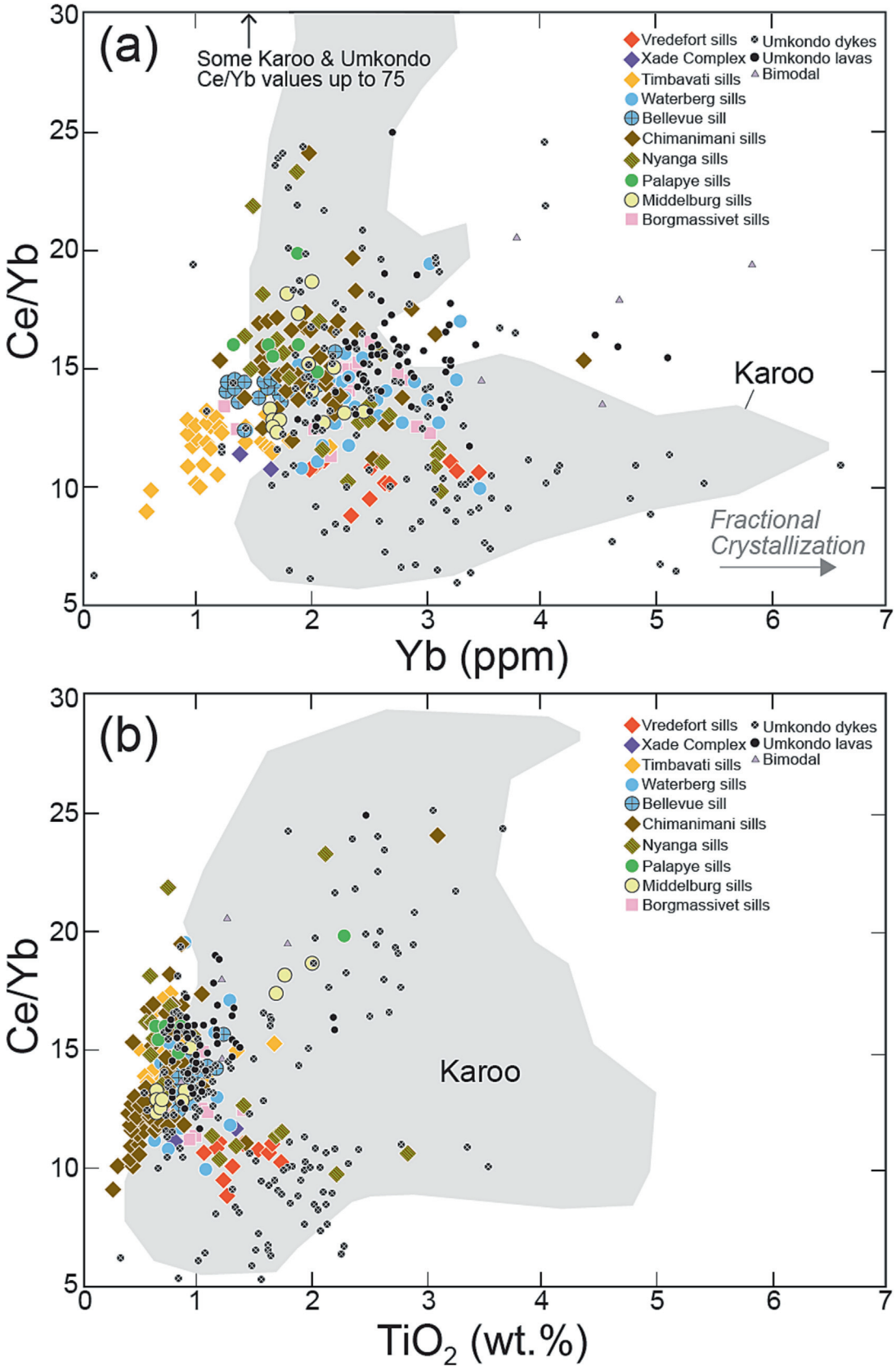


Fig. 5. (a) Ce/Yb versus Yb. The Umkondo province typically has greater Ce/Yb compared to the Karoo province (grey field). (b) Ce/Yb versus TiO_2 (wt.%). The Karoo province has a greater number of rocks with high TiO_2 contents (>1.5 wt.%) compared to the Umkondo province, which is mostly characterised by low TiO_2 contents (<1.5 wt.%).

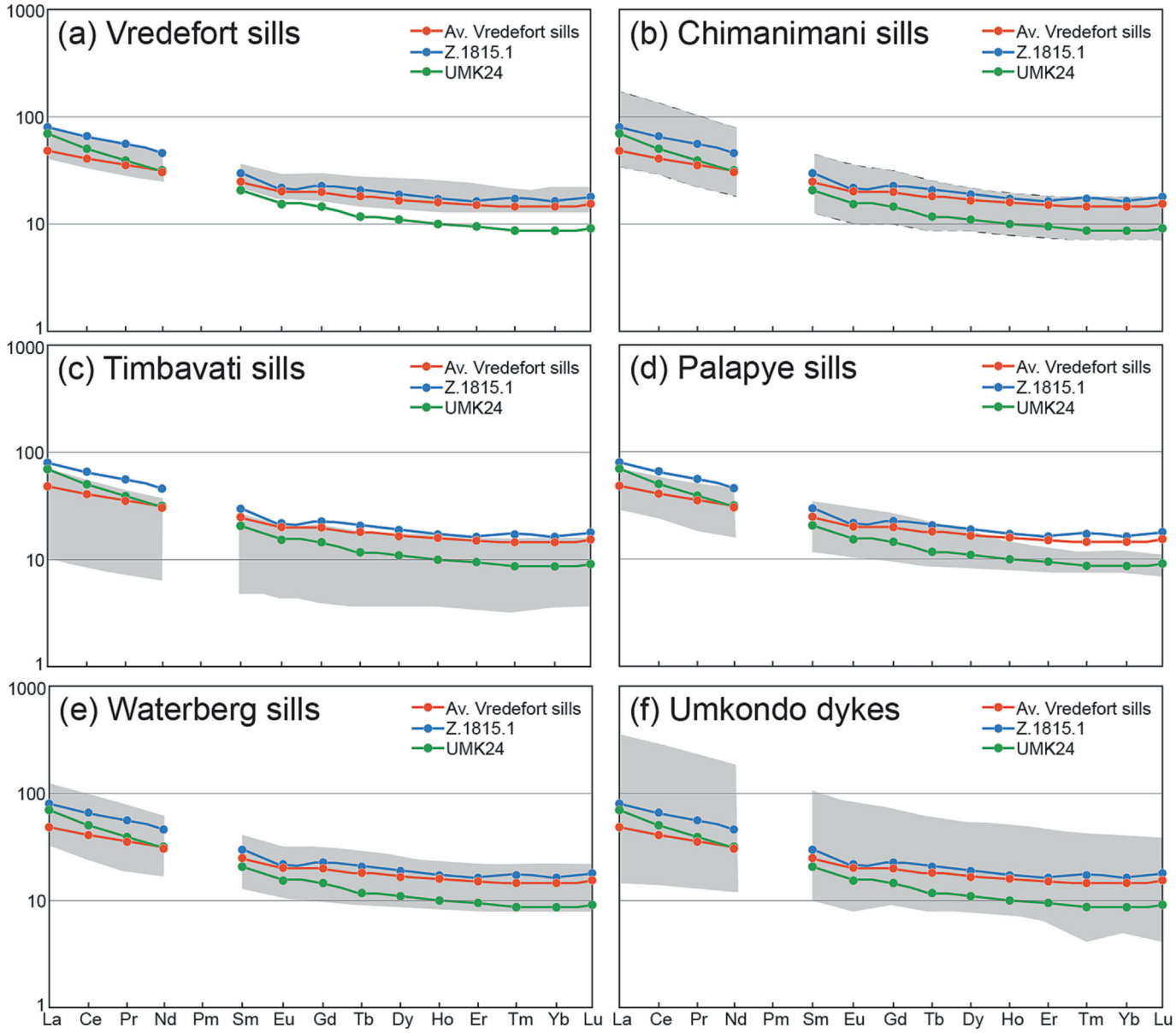


Fig. 6. Rare Earth Element diagrams of selected domains in the Umkondo province normalized to Chondrite values (C1: McDonough and Sun, 1995). (a) Vredefort sills; (b) Chimanimani sills; (c) Timbavati sills; (d) Palapye sills; (e) Waterberg sills; and (f) Umkondo dykes (all are shown as grey fields). The average Vredefort sill composition, a Borgmassivet sill composition (sample Z.1815.1) and a Chimanimani sill (UMK24) are also shown for comparison.

The Espungabera and Straumsnutane lavas have similar εNd isotopic compositions to the Borgmassivet, Timbavati and Waterberg although the Straumsnutane lavas show a wider range of initial $^{87}Sr/^{86}Sr$ with a low value (0.701627) and more elevated values (>0.72) because of secondary alteration (Fig. 8a). The Umkondo dykes show the widest ranges of isotopic compositions with some of the most enriched and depleted values in the entire Umkondo province (initial $^{87}Sr/^{86}Sr$ of 0.703008 to 0.757554 and εNd of 7.4 to −15.6). The Mutare and Kamativi dykes have the most radiogenic εNd (up to 7.3), whereas the Guruve dykes have the least radiogenic εNd (up to 1). The most unradiogenic εNd values are in the Mahoba dykes of India (−11). Some of the Sr-Nd isotope compositions for the dykes are comparable to the Vredefort sills (Fig. 8a). The εNd values (at 1.11 Ga) for the Umkondo sills show a strong correlation with Ce/Yb such that those samples with the most unradiogenic Nd isotopic compositions have the highest Ce/Yb (Fig. 8b). The Vredefort sills and Xade Complex show the lowest Ce/Yb at relatively more radiogenic Nd isotopic compositions (Fig. 8b).

6. Discussion

6.1. Umkondo magmatism initiated by a mantle plume

The Umkondo province is distributed across southern Africa and the recent discovery of Umkondo-age dykes in southern Angola (Salminen et al., 2018) extends its spatial coverage to > 2 Mkm^2 (Fig. 1). This makes the Umkondo province comparable in size and volume (~2 Mkm^3) to the significantly younger Karoo province. High-precision U-Th-Pb dating of zircons and baddeleyite extracted from dolerite sills across the Umkondo province reveals that it was emplaced over a relatively short duration of 3–5 million years (Hanson et al., 2004) and which is comparable to the Karoo

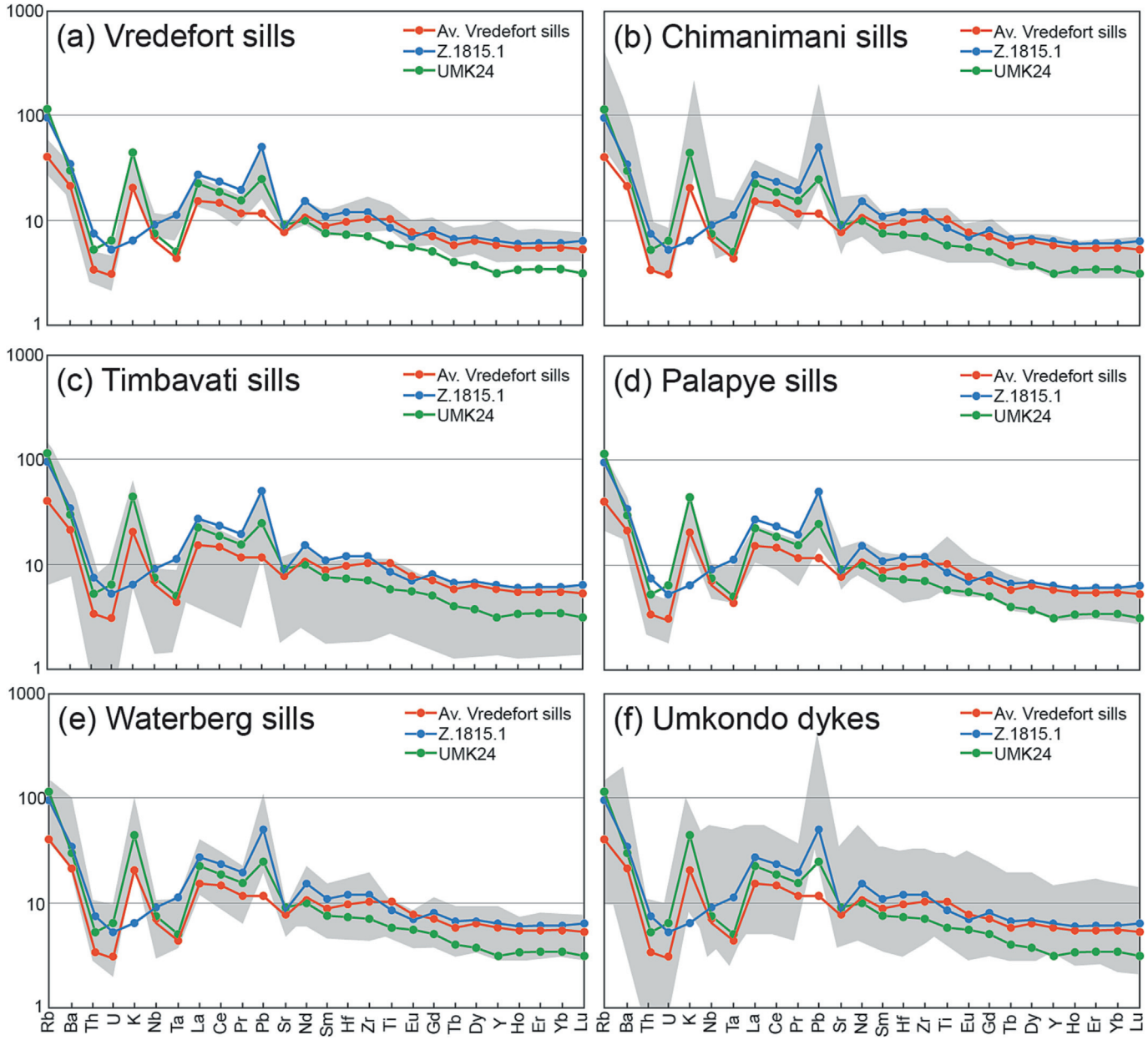


Fig. 7. Multi-element diagrams of the Umkondo province normalized to Primitive Mantle values (Sun and McDonough, 1989). (a) Vredefort sills; (b) Chimanimani sills; (c) Timbavati sills; (d) Palapye sills; (e) Waterberg sills; and (f) Umkondo dykes (all are shown as grey fields). The average Vredefort sill composition, a Borgmassivet sill composition (sample Z.1815.1) and a Chimanimani sill (UMK24) are also shown for comparison.

province (Svensen et al., 2012; Muedi et al., 2022). This rapid rate of emplacement, its large volume, and the distribution of some of its products near the boundary of the Kalahari craton (Fig. 1) are the widely regarded geological characteristics of basaltic magmatism initiated by a mantle plume (e.g., Ernst, 2014). We, therefore, suggest that Umkondo magmatism was initiated by a mantle plume at 1.11 Ga.

Interestingly, the timing of Umkondo magmatism broadly coincides with the assembly of the Rodinia supercontinent (Hanson et al., 2004; Coltice et al., 2009; de Kock et al., 2014). Because of this, an alternative explanation to a mantle plume for Umkondo magma production was proposed by de Kock et al. (2014), in which continental aggregation led to the thermal insulation of the mantle as well as an enlarged wavelength of mantle convection, resulting in mantle melting (as proposed in Coltice et al., 2009). However, as pointed out by de Kock et al. (2014), this alternative model is heavily dependent on the palaeogeography of the Kalahari craton for which there are currently few constraints. Until there are better constraints on the timing of Rodinia assembly and its paleogeographic configuration, the thickness of the crust-lithosphere at 1.11 Ga, and the tectonic setting of the Umkondo province, we explain the origin of Umkondo magmatism by plume-induced mantle melting beneath the Kalahari craton. This is on the basis of the compositional systematics of the Umkondo magmas using both existing and new geochemical datasets, their compositional evolution, and the role of the lithosphere in modifying the primary chemical signatures of the melts.

6.2. Low-Ti continental tholeiites in the Umkondo province

Continental flood basalt provinces are characterised by geochemical patterns influenced by either melting of enriched mantle

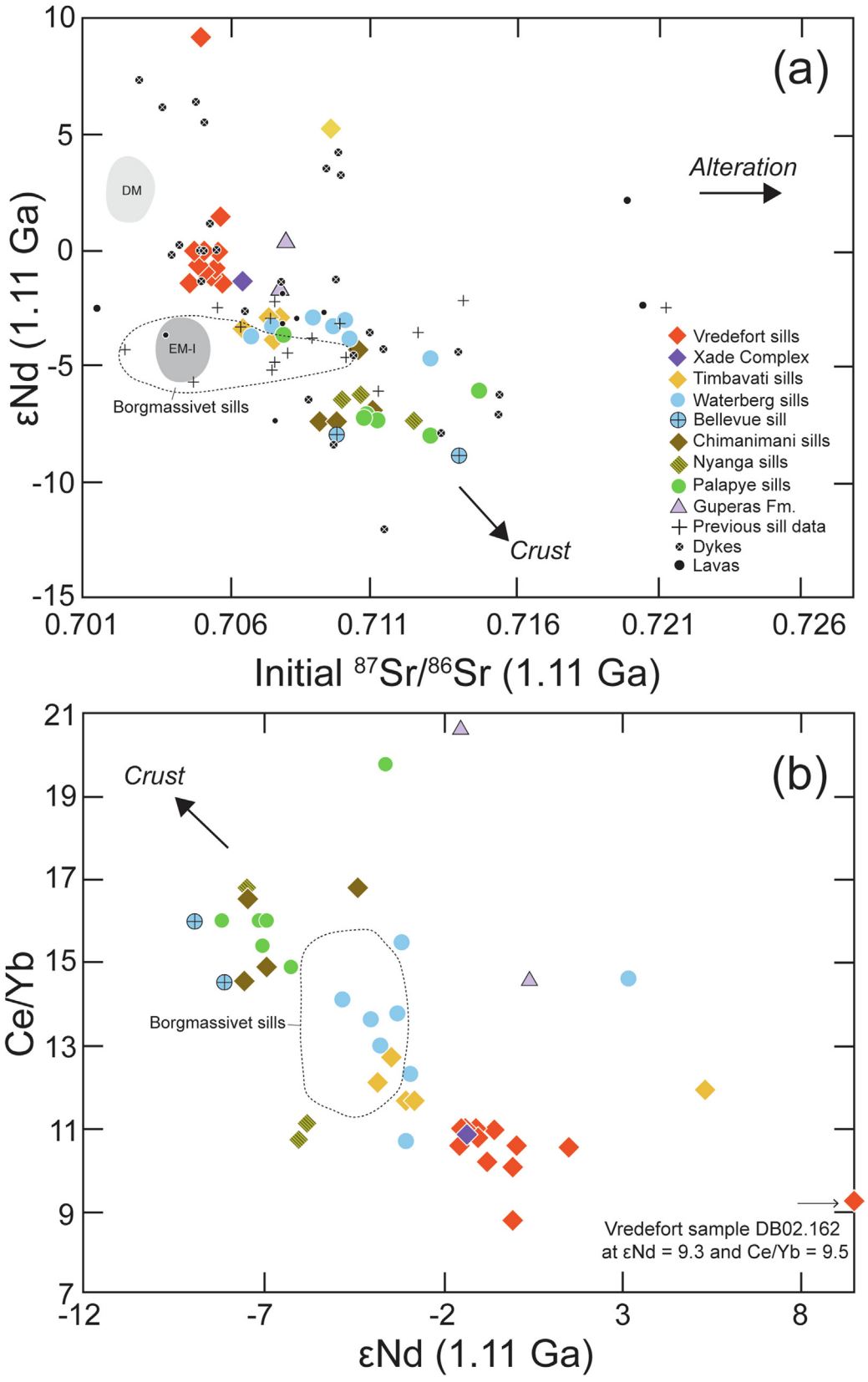


Fig. 8. (a) εNd versus initial $^{87}Sr/^{86}Sr$ (age-corrected to 1.11 Ga) for the various suites of sills in the Umkondo province. The field defined by the dotted line represents the extent of the Borgmassivet Sr-Nd isotopic data (Riley and Millar, 2014). Previous Sr-Nd isotopic data for Umkondo sills (Bullen, 2005; Bullen et al., 2012), dykes (Ward, 2002; Choudhary et al., 2019) and lavas (Moabi et al., 2015, 2017) are also included. The approximate locations of the depleted mantle (DM) and enriched mantle-I (EM-1) at 1.11 Ga are shown. (b) εNd (1.11 Ga) vs. Ce/Yb for our new dataset for the Umkondo province.

sources (sublithospheric or lithospheric mantle) or the interaction of sublithospheric mantle-derived magmas with enriched lithospheric mantle or crust (Ernst, 2014). The Umkondo province was emplaced onto the Kalahari craton during the Mesoproterozoic and its various domains were emplaced into Proterozoic sedimentary sequences and Archean granite-gneisses (Hanson et al., 2004, 2006). The tectonic setting of the Umkondo province is comparable to other intra-continental tholeiitic provinces (Ernst, 2014) and the chemistry of the magmas was likely to have been modified by lithosphere and/or crust during their emplacement.

Since early studies on the Karoo province, it has been recognised that continental flood basalt provinces may be subdivided into high- and low-Ti suites (Cox et al., 1967). This subdivision has been applied to continental flood basalts globally (e.g., Xu et al., 2004; Jourdan et al., 2007; Shellnutt, 2014). The Umkondo province is characterised mainly by low-Ti magmas (Fig. 5b). There are few Umkondo dyke compositions that may be representative of a high-Ti magma suite (>1.5 wt.% TiO_2; Fig. 5b). High and low-Ti magmas are spatially restricted in some basaltic provinces and such "geochemical provinciality" is thought to be controlled by the interaction between rift systems and mantle plume impingement (Xu et al., 2004; Jourdan et al., 2007; Ashwal, 2021). This is evident in the Karoo province with a triple junction (i.e., plume impingement site) apparent on spatial-geochemistry maps (Ashwal, 2021). We plotted the distribution of low-Ti and high-Ti magma suites for the Umkondo province and observed no comparable distribution to the Karoo province (not shown here). High-Ti magmas are, however, volumetrically insignificant in the Karoo province compared to the low-Ti magmas (Ashwal, 2021) and their paucity in the Umkondo province may simply be explained by their lack of preservation in this substantially older province.

The Umkondo province has incompatible trace element profiles that are typical of continental flood basalt provinces, and which can be attributed to either crustal or lithospheric mantle contamination. Typical signatures include negative Nb-Ta, positive Ti-K-Ba-Rb, and enrichment in light/heavy REE (Fig. 7). Low Nb-Ta is common in continental flood basalt provinces and is also a distinct feature of continental arcs and evolved island arc volcanic rocks. Low Nb-Ta may be attributed to the incorporation and retention of these metals in minor Ti-rich phases such as rutile and titanite, as slab-derived fluids are selectively enriched in LILE during subduction (Saunders et al., 1988). This has also been suggested as an explanation for the low Nb-Ta in the Karoo province (Elburg and Goldberg, 2000; Jourdan et al., 2007). Low Nb-Ta in the magmas can be explained by either melting of the continental lithospheric mantle or the melting of the asthenospheric mantle infused with components of recycled oceanic lithosphere.

6.3. Compositional evolution of the Umkondo magmas

The major element oxides of the Umkondo province are all relatively evolved in composition compared to primary magmas produced from the mantle. Some of the most magnesian sills contain > 7 wt.% MgO and are derivatives of primary magmas after olivine-only fractionation (Fig. 3a). We performed a series of fractional crystallization models using rhyolite-MELTS (Gualda et al., 2012; Ghiorso and Gualda, 2015) for the most primitive magma compositions to forward model their liquid line of descent and to see if they replicated the natural data. The best-fit models shown in Fig. 3 are at 1 kbar pressure and an oxygen fugacity at QFM + 1 (and QFM-1) with H_2O contents of 0 wt.% (and 1 wt.%).

Our most primitive composition in the Umkondo dataset is a Nyanga sill (sample UMK24 with 12.37 wt.% MgO). The fractional crystallization of UMK24 produces a liquid line of descent that fits the lower part of the natural Umkondo data (blue dashed line in Fig. 3). Another primitive magma composition is represented by a Borgmassivet sill (sample Z.1815.1 with 11.48 wt.% MgO). The major element oxide trends of almost the entire Umkondo province can be explained by low-pressure (1 kbar) fractional crystallization of a parent magma represented by Z.1815.1 (green dashed line in Fig. 3). Fractional crystallization of a less primitive magma from the Vredefort sills (sample DB02.162 with 8.62 wt.% MgO), produces a liquid line of descent that fits parts of the natural Umkondo data (brown dashed line in Fig. 3). In each of the models, the co-crystallisation of plagioclase and clinopyroxene decreases Al_2O_3 and CaO and increases FeO^t at melt MgO contents of 6–7 wt.%. As melt compositions approach 4 wt.% MgO, there is a decrease in FeO^t-TiO_2 that corresponds to the crystallization of Fe-Ti oxides. The overall enrichment in SiO_2 produces granitic melt compositions that are comparable to the compositions of the granophyre present in the thicker Umkondo sills (Fig. 3). The rhyolite compositions in the Guperas Formation and Kgwebe-Ghanzi-Chobe rift may either be differentiated products of Umkondo basalt fractionation, or they are the products of crustal melting induced by Umkondo plume magmatism (Fig. 3). More detailed isotopic studies of these rhyolites are required to constrain their petrogenesis and possible relation to the Umkondo province. Continental large igneous provinces typically contain the entire spectrum of volcanic and plutonic siliceous rock types (Ernst, 2014). Incidentally, some of the models (for samples Z.1815.1, DB02.162, and UMK24) fit some of the low FeO-MgO compositions at QFM-1 and 1 wt.% H_2O and this may suggest that some of these magma compositions may have been contaminated at a late stage.

Collectively, the fractional crystallization models of samples Z.1815.1, DB02.162 and UMK24 bracket the natural Umkondo data. This shows that the Umkondo province basalts are products of three-phase fractional crystallization of oxidised parent magmas with $\sim$ 10 wt.% MgO at pressures of 1 kbar. The shallow pressures are consistent with the typical tectonic setting of the Umkondo sills in terms of their emplacement into high-level Paleoproterozoic sedimentary successions, some of which may have been wet and semi-lithified (Munyanyiwa, 1999; Riley and Millar, 2014). The depth of emplacement of the Umkondo intrusions that were intruded into Archean granite-gneisses, such as the Vredefort, Timbavati and Nyanga sills, is more difficult to constrain. It may be that these sills crystallized at greater pressures in the mid-crust as implied by the presence of abundant orthopyroxene in the Timbavati sills. To test this, we performed fractional crystallization models at greater pressures of 2–3 kbar. There are minor differences in the higher-pressure models compared to the lower-pressure models (1 kbar) including the later onset of plagioclase-clinopyroxene crystallization. None of the higher pressure models can better explain the array of Vredefort, Timbavati and Nyanga sill compositions compared to the 1 kbar models. There are also subtle differences in the major element compositions of the parent magmas to the Umkondo province, as indicated by there being no good model match to the natural data. These variations in major element compositions may be a product of lithological variations in the mantle source.

6.4. The composition of the primary magmas and a lack of ultramafic cumulates

The Umkondo province is mostly composed of low-Ti basalt to basaltic-andesite rocks with moderate MgO contents (average MgO is 8 wt.%, n = 640). The Umkondo samples with MgO contents > 8 wt.% are present in the Waterberg, Borgmassivet, Vredefort, Chimanimani, Nyanga and Palapye sills (Fig. 3). We do not have much petrological information on the dykes, so some of their elevated MgO contents (>10 wt.% MgO) may be caused by the accumulation of ferromagnesian minerals. We selected some of the most MgO-rich samples for inverse models to determine the primary

magma composition. These included samples from the Vredefort and Borgmassivet sills as they are some of the least evolved MgO-SiO_2 compositions (Fig. 3) and the lowest Ce/Yb (Fig. 5a).

We used PRIMELT3 to calculate the composition of the primary magmas in the Umkondo province, assuming its parent magmas were previously subject to olivine-only extraction (Herzberg and Asimow, 2015). Sample Z.1815.1 of the Borgmassivet sills contains 48.7 wt.% SiO_2 and 11.5 wt.% MgO and it also contains the lowest Al_2O_3 and highest CaO concentrations (Riley and Millar, 2014). This is a composition that is relatively primitive and is plausibly related to the primary magma composition by olivine-only addition. PRIMELT3 shows that Z.1815.1 is the product of 40% partial melting of garnet peridotite, consistent with covariations of Zr/Nb-Ce/Y (Riley and Millar, 2014). The estimated primary magma composition contains 18.5 wt.% MgO (in equilibrium with mantle olivine of Fo_{90}) and ~ 21% olivine extraction is required from this primary magma to produce a magma with the MgO composition of Z.1815.1. We attempted to estimate the primary magma in equilibrium with sample DB02.162 (MgO of 8.6 wt.%), the most magnesian Vredefort sill. However, this sample failed the source test as it may be derived from an olivine-free (i.e., pyroxenite) source (Herzberg and Asimow, 2015). This caveat results in a larger error margin of 2–3 wt.% MgO and an overestimation of the mantle potential temperature by ~ 50–70 °C. Nevertheless, the primary magma in equilibrium with mantle olivine (Fo_{90}) estimated for the Vredefort sills has MgO contents of 19 wt.% with ~ 33% olivine extraction required. Although the Vredefort inverse model is less reliable than that for Z.1815.1 (a Borgmassivet sill), the results are comparable. UMK24 of the Nyanga sills also failed the source test as it may also have a pyroxenite source. The calculated primary magma for UMK24 contained 16.4 wt.% MgO with less olivine extraction required (~12%), as is expected because of the greater MgO contents (12.4 wt.%) of UMK24.

Our models using PRIMELT3 indicate that the primary magmas in the Umkondo province are komatiitic with high estimated mantle potential temperatures of 1660 °C. This lends support to our view that Umkondo magmatism was triggered by a mantle plume. Most of the compositions in our compiled database for the Umkondo province are therefore basalts representing residual melts after olivine-only crystallization of primary komatiitic magmas.

Despite the evidence for a komatiitic primary magma, there is a dearth of ultramafic cumulates preserved in the Umkondo province. The Timbavati sills are some of the few ultramafic rocks in the entire Umkondo province. The Timbavati sills have some of the highest MgO contents (up to 29 wt.%) and petrographic observations on these rocks reveal that the MgO enrichment is controlled by olivine (and orthopyroxene) accumulation (Bullen, 2005). The Xade Complex also contains cumulate rocks of peridotite and pyroxenite. Further investigation of the Xade Complex and the Timbavati sills is required to see if their cumulate rocks are derived from primary komatiitic magmas. We postulate that the komatiitic primary magmas to the Umkondo province may have stalled and fractionated in the deeper crust or a Moho-level sill complex (Cox, 1980). High-velocity zones in the lower crust that correspond to dense ultramafic cumulates may be recognised in geophysical techniques, although it would be a challenge to distinguish underplated material associated with the Umkondo province from other major magmatic provinces that developed on the Kaapvaal craton (Cole et al., 2021).

6.5. Crustal and lithospheric processes during Umkondo magmatism

6.5.1. Crustal and/or lithospheric mantle contamination of the primary magmas

The geochemistry of continental flood basalts globally reflects some amount of magma interaction with the lithospheric mantle and/or the continental crust. In comparison to the Umkondo province, there is a vast combined Sr-Nd isotope dataset for the Karoo province (Ashwal, 2021). Nevertheless, the low-Ti rocks of the Umkondo province have comparable isotopic signatures to the low-Ti rocks of the Karoo province, showing a broad range of Sr-Nd isotope compositions consistent with continental crust and/or lithospheric contamination of mantle-derived magmas (Fig. 8a) as is supported by the correlation with Ce/Yb (Fig. 8b). However, distinguishing between crustal and lithospheric mantle reservoirs is challenging, although there are trace element variation diagrams that can be used to gain some insight into their relative contributions (e.g., Pearce, 2008; Pearce et al., 2021).

On a Th/Yb-Nb/Yb diagram, the Umkondo province plots almost entirely above the MORB-OIB array and is consistent with contamination of the magmas either by the lithospheric mantle or the continental crust (Fig. 9a). The Vredefort and Timbavati sills (and some of the Umkondo dykes) are generally closer to the depleted mantle-OIB array and represent some of the least contaminated magmas (Fig. 9a). This is consistent with the Sr-Nd isotopes for these sills (Fig. 8a). The Chimanimani and Nyanga sills of eastern Zimbabwe show some of the highest Th/Yb-Nb/Yb (Fig. 9a) that is consistent with the enriched Sr-Nd isotope data for these sills (Fig. 8a). This suggests to us that the Umkondo sills of eastern Zimbabwe record significant amounts of crustal and/or lithospheric mantle contamination. This is further supported by covariations in Nb/La-Ce/Sm (Fig. 9b) and ΔNb-La/Nb (Fig. 10b).

Based on (i) negative Nb-Ta anomalies in the Umkondo province, (ii) Sm-Nd model ages of 1950–2142 Ma, and (iii) evidence from xenoliths of a diverse subcontinental lithospheric mantle in southern Africa, it was argued that the parent magmas to the Waterberg sills were derived from the sublithospheric mantle but were contaminated by the lithospheric mantle (Bullen et al., 2012). A similar petrogenetic model was proposed for the Borgmassivet sills (Riley and Millar, 2014). Depletion in HFSE, enrichment in LILE, and enriched isotopic compositions are also all evident chemical signatures in the Karoo province. Karoo magmas similarly show evidence of magma-crust/lithosphere interaction, but a greater amount of Karoo data plot at lower Th/Yb (Fig. 9) and may therefore be less contaminated than the Umkondo province (also consistent with their lower Ce/Yb; Fig. 5a). Alternatively, this may simply be explained by the Umkondo province having assimilated significantly older and more enriched crustal material compared to the Karoo province, which is apparent in the relationship between Ce/Yb and εNd (Fig. 8b).

In conclusion, we concur with the suggestions from previous studies on certain domains in the Umkondo province that its magmas are derived from the sublithospheric mantle and that there was subsequent crustal and/or lithospheric contamination involved in their petrogenesis. Distinguishing between these two continental reservoirs is challenging. Given the evidence presented above that the primary magmas to the Umkondo province were komatiitic and that these primary magmas fractionated in the deep crust, there would have been ample opportunity for these hot primary magmas to assimilate more enriched crustal material. This culminated in the emplacement of fractionated and contaminated basalts in the shallow crust of the Kalahari craton.

6.5.2. Evidence of crystal-melt separation

Most Umkondo sills are sub-ophitic to ophitic doleritic-gabbros without macroscopic modal layering. There is, however, well-developed orthopyroxene-olivine modal layering in the Timbavati sills (Bristow et al., 1982; Bullen, 2005) and this is apparent in the major element variation diagrams (Figs. 3 and 4). Least-squares regression of bulk rock MgO-FeO compositions in the Timbavati sills shows that there was the accumulation of $Fo_{87\text{-}86}$ olivine. The presence of orthopyroxene primocrysts in the Timbavati sills

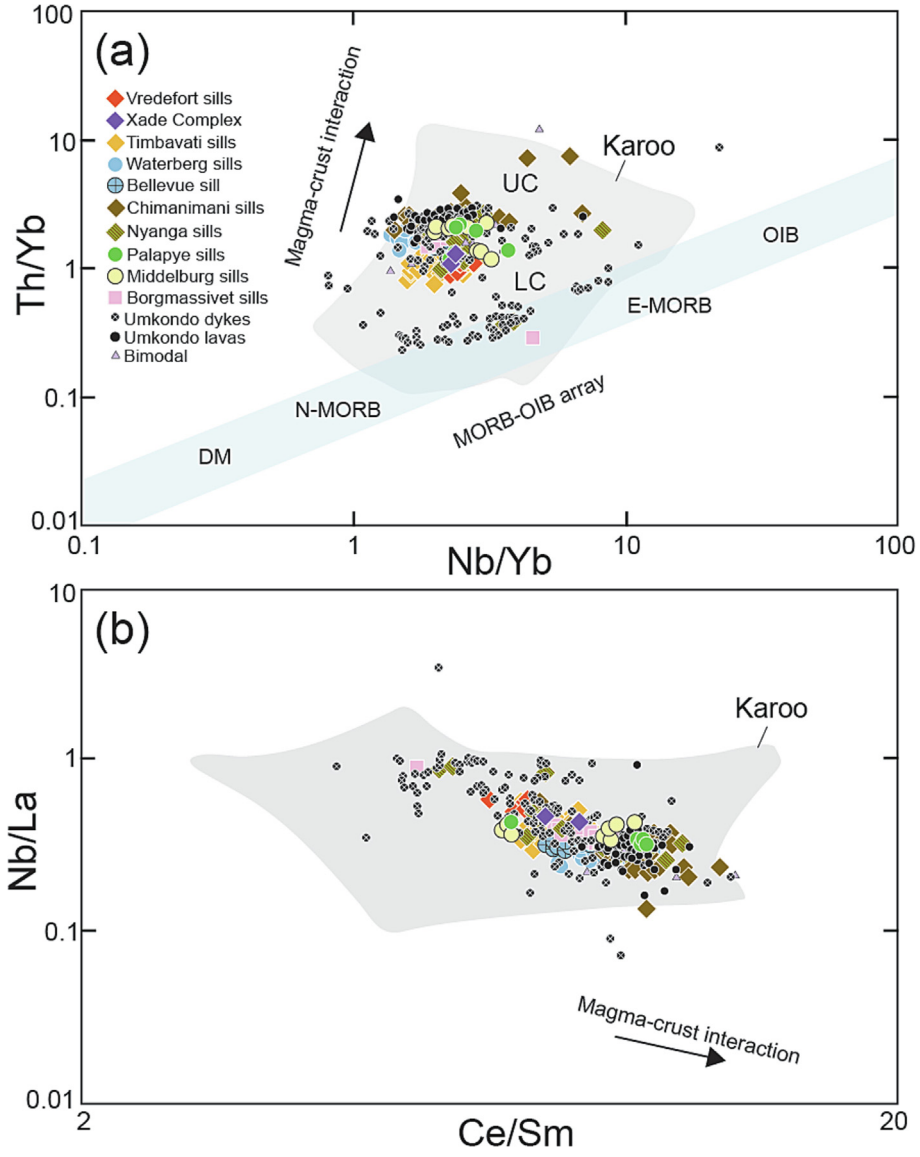


Fig. 9. (a) Th/Yb versus Nb/Yb for the Umkondo province (after Pearce, 2008). Th/Yb is a proxy for crustal input and Nb/Yb is a proxy for the melting % and source composition. The MORB-OIB array is shown (DM = Depleted Mantle; N-MORB = Normal MORB; E-MORB = Enriched-MORB; OIB = Ocean Island Basalt; UC = Upper Crust; LC = Lower Crust). (b) Nb/La versus Ce/Sm for the Umkondo province showing evidence of magma and crust interaction. The Karoo province (grey field) is included for comparison.

may mean that this predicted equilibrium olivine composition is overestimated. This appears to be the case, as measured compositions of olivine in the Timbavati sills are slightly lower (Fo_{83-68}) than the predicted olivine Fo compositions (Bullen, 2005). Olivine with compositions of Fo_{87-86} would be in equilibrium with melt MgO contents of ~ 13–14.5 wt.% (Matzen et al., 2011). These melt compositions are more primitive than the majority of the Umkondo sills but are fractionated compared to the modelled primary melt composition of ~ 18 wt.% MgO. Further studies on the mineral compositions of the Timbavati sills are required to unravel their petrogenesis.

There is also modal layering in the Borgmassivet sills (Riley and Millar, 2014) and the Xade Complex, and nearby Tshane and Tsetseng Complexes, are large layered mafic–ultramafic intrusions (Corner et al., 2012). These intrusions may represent large reservoirs of Umkondo magma that were periodically replenished and had time to fractionate. There is widespread development of mm to cm-sized granophyric segregations in many of the Umkondo sills that are consistent with fractional crystallization to granitic melt compositions. Many of these granitic segregations can be explained by fractional crystallization of parent Umkondo magmas (e.g., Fig. 3). The Umkondo lavas have similar Ce/Yb and greater concentrations of Yb to the Umkondo sills (Fig. 5a). This suggests to us that the lavas are generally more evolved than the sills and they may have been sourced from either relatively more fractionated parts of the Umkondo sills or deeper, more fractionated parts, of the Umkondo magmatic plumbing system.

Because of the dearth of picritic and komatiitic compositions in the Umkondo province, we suggest there was significant processing (e.g., magma storage, fractional crystallization, and crystal accumulation) in the deeper crust before the emplacement of Umkondo magmas in the shallow crust.

6.6. Mantle source(s) to the Umkondo province

The magma sources of continental flood basalts have been a controversial subject for a number of decades (e.g., Gallagher and Hawkesworth, 1992; Arndt et al., 1993; Wooden et al., 1993;

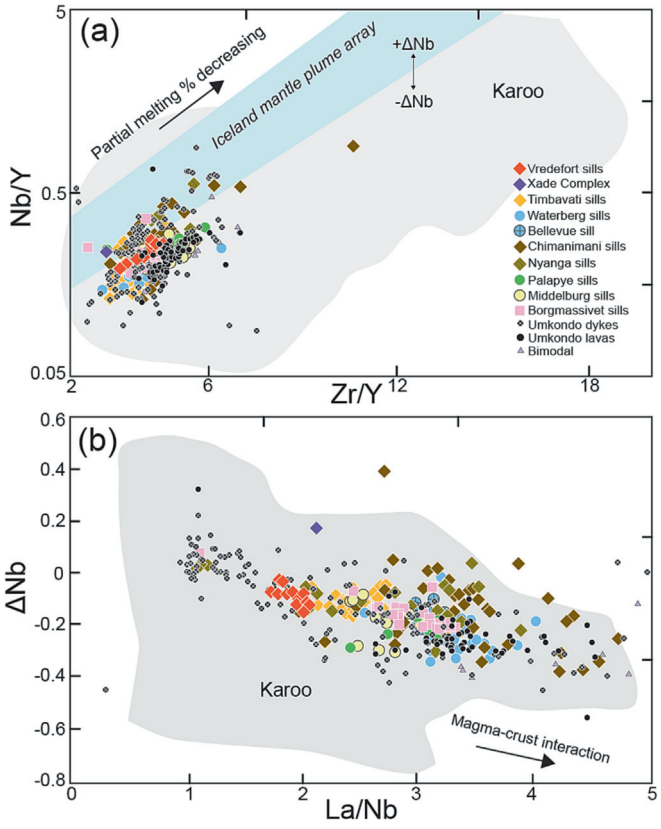


Fig. 10. (a) Nb/Y versus Zr/Y for the Umkondo province with the arrows indicating whether there is a deficiency in ΔNb (after Luttinen, 2018). (b) ΔNb versus La/Nb showing evidence of lithospheric and/or Kaapvaal crust interaction in the Umkondo province. The Karoo province (grey field) is shown for comparison.

Jourdan et al., 2007; Sobolev et al., 2007; Beard et al., 2017; Ashwal, 2021; Bédard et al., 2021). The potential sources of magmas include the sublithospheric mantle (i.e., the convecting asthenosphere or the mantle plume) and the subcontinental lithospheric mantle. We argue that (i) the sheer volumes of magma that formed the Umkondo province (>1 Mkm^3), (ii) the komatiitic composition of the primary magmas (~18 wt.% MgO), and (iii) the high mantle potential temperatures of the primary magmas (>1660 °C), preclude an origin from the subcontinental lithospheric mantle and that the most significant mantle source was the sublithospheric mantle beneath the Kalahari craton. We now provide constraints on the composition of the sublithospheric mantle source.

6.6.1. High Ce/Yb and low Sm/Yb Umkondo magmas and shallow melting of spinel lherzolite

The low-Ti tholeiites of the Umkondo province generally have high Ce/Yb and similar light/heavy rare earth element enrichment is documented in continental flood basalt provinces elsewhere (e.g., Beard et al., 2017; Bédard et al., 2021). Even the average Ce/Yb of the Umkondo province (Ce/Yb = 13) is high compared to the low-Ti tholeiites of the Karoo province (Ce/Yb = 7). The average Ce/Yb of the least contaminated Umkondo sills (Ce/Yb = 10 for Vredefort, Timbavati and Borgmassivet sills; Fig. 5a) is higher than the Karoo province. The trend to high Ce/Yb is apparent in the Chimanimani, Nyanga and Palapye sills, and coupled with their Sr-Nd isotopic compositions (Fig. 8a), it is likely to have been controlled by the assimilation of light rare earth element-enriched crustal materials. Despite high Ce/Yb, the Umkondo sills show limited fractionation of heavy rare earth elements (Sm/Yb = 2), and non-modal melting paths indicate up to 2%–20% melting of a spinel lherzolite mantle source (Fig. 11). Melting depths of 40–50 km in the Umkondo province are estimated using Sm/Yb (Dockman et al., 2018). The shallowest melting depths are ~ 15 km and are commonly recorded in the Umkondo dykes and more rarely in the Waterberg and Timbavati sills. There is limited evidence in the Umkondo province of deep (>50 km) mantle melting. The deepest melting depths estimated using Sm/Yb are ~ 70 km and are restricted to high-Ti Umkondo dykes.

6.6.2. Evidence of a heterogeneous sublithospheric mantle source

A sublithospheric mantle source and subsequent crustal and/or lithospheric mantle contamination model has been proposed for the Umkondo province (e.g., Bullen et al., 2012; Riley and Millar, 2014). Zn/Fe-MgO relations in Fig. 13 suggest there was some contribution from pyroxenite source material that was possibly an enriched-MORB (E-MORB) like mantle source. Sr-Nd isotopes also support a contribution from enriched mantle sources as they extend from the depleted mantle (DM) and enriched mantle (EM-I) endmembers (Fig. 8a) and this is further supported on a plot of TiO_2/Yb-Nb/Yb that indicates E-MORB sources (Fig. 12). The Umkondo province forms an array that extends to low TiO_2/Yb and low Nb/Y values. This is very similar to the Karoo province, although there is greater evidence of deeper ocean island basalt (OIB) melting depths in the Karoo province. Only a few Umkondo samples show evidence of deeper melting (Fig. 12). The samples with the lowest TiO_2/Yb-Nb/Yb in the Umkondo province are in the Waterberg and Palapye sills (Fig. 12) and this is consistent with their more enriched Sr-Nd isotopic compositions (Fig. 8). These enriched compositions are because of crustal and/or lithospheric mantle contamination. The Vredefort sills and Xade Complex show the most depleted Sr-Nd isotopic compositions and lowest Ce/Yb and sit between the DM and EM-I endmembers (Fig. 8a). The Borgmassivet sills in part overlap with the field of EM-I and have slightly more unradiogenic Nd isotopic compositions compared to the Vredefort sills (Fig. 8a). This is consistent with the slightly higher Ce/Yb values in the Borgmassivet sills compared to the Vredefort sills (Fig. 8b). In summary, there is evidence that the Umkondo magmas are derived from enriched mantle sources.

It is apparent from the trace element discrimination diagrams (e.g., Fig. 9) and the Sr-Nd isotopes (Fig. 8a) that the enriched mantle source was variable in composition. Evidence for compositional variability is also apparent in the PRIMELT3 models. The Borgmassivet sills have major element compositions that are consistent with magma derivation from a peridotite source and the Vredefort sills have major element compositions that are consistent with magma derivation from a pyroxenite source. We investigated this further using the Zn/Fe calibration of Le Roux et al. (2010). Clinopyroxene and garnet-bearing sources are characterised by low Zn/Fe compared to the coexisting melt, olivine and orthopyroxene. This partitioning behaviour implies that Zn/Fe is not fractionated during the partial melting of peridotite (assuming differentiation is controlled by olivine-only fractionation). High Zn/Fe of some OIB cannot be explained by the melting of peridotite alone and requires the presence of high Zn/Fe lithologies such as eclogites and pyroxenites (Le Roux et al., 2010). On a diagram of Zn/Fe ($\times 10^4$)-MgO, the Umkondo province has mostly peridotite sources with minor contributions of pyroxenite (Fig. 13). This distribution is comparable to the Karoo province in which pyroxenite sources have been recognized (e.g., Heinonen et al., 2013; Howarth and Harris, 2017). There is also evidence for the preservation of Umkondo magmas derived from pyroxenite sources in the Waterberg, Middelburg, Chimanimani, and Nyanga sills as well as the dykes (Fig. 13). The Zn/Fe relations are corroborated by our inverse PRIMELT3 models. Sample UMK24 of the Nyanga sills is derived from a pyroxenite source and sample DB02.97 of the Timbavati sills is derived from a peridotite source. However, samples DB02.26 and

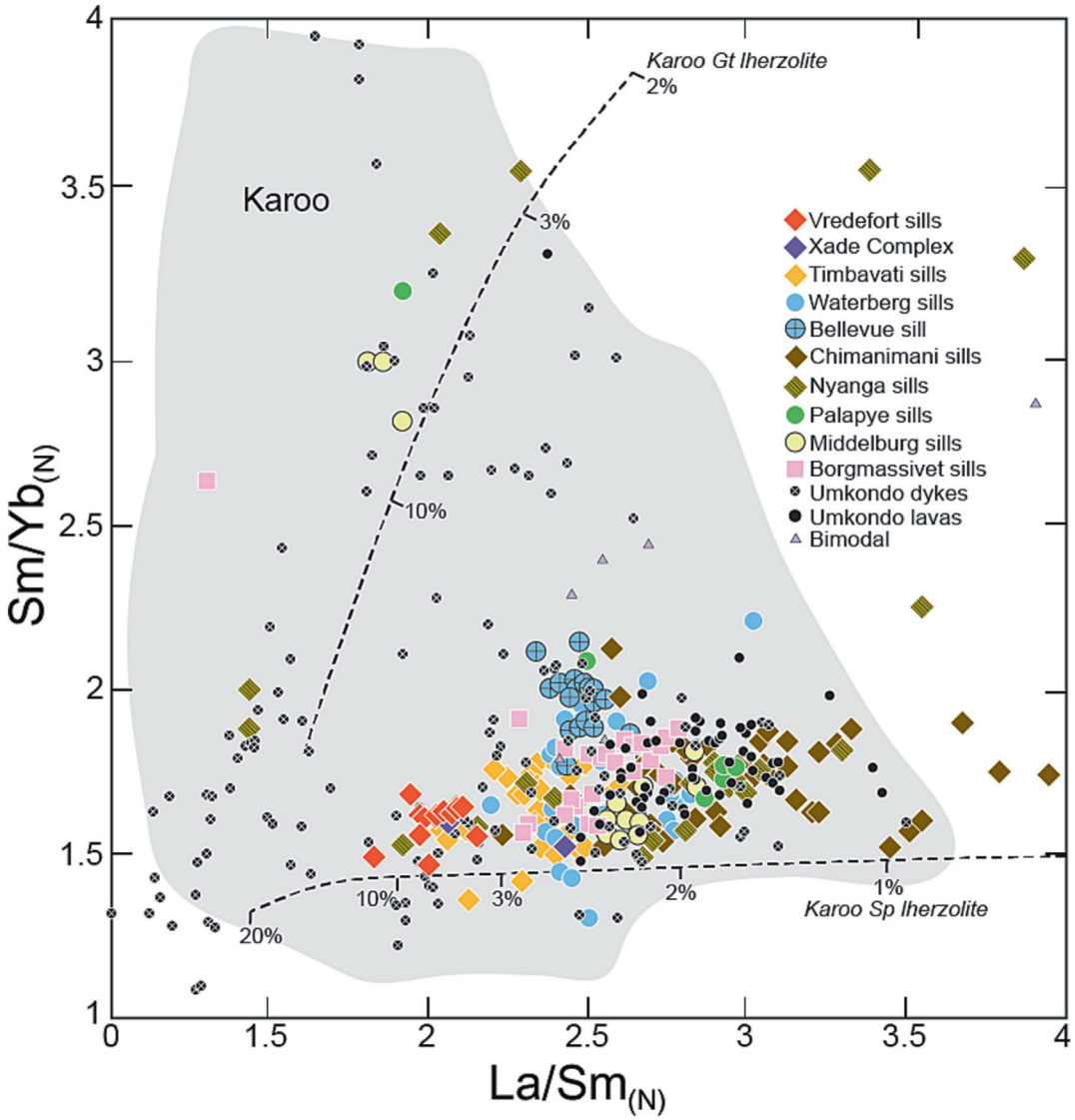


Fig. 11. Sm/Yb versus La/Sm (both normalised to Primitive Mantle values of Sun and McDonough, 1989) for the Umkondo province. The spinel lherzolite and garnet lherzolite melting paths for Karoo sources are shown (taken from Bédard et al., 2021).

DB02.76 are other liquid-like compositions in the Timbavati sills, and they only have slightly greater Zn/Fe than sample DB02.97 and are derived from pyroxenite sources. The Borgmassivet sills and their counterpart Straumsnutane lavas are in the peridotite source field, which is consistent with the inverse PRIMELT3 model for sample Z.1815.1. It should be noted that the samples with the lowest Ce/Yb in the Vredefort and Borgmassivet sills, as well as the Xade Complex, all have low Zn/Fe, and are therefore mostly derived from peridotite mantle sources.

Olivine in the Timbavati sills has low CaO (0–0.2 wt.%) and may also be consistent with the derivation of its magmas from pyroxenite sources (Bullen, 2005). Although Mn/Fe of olivine is high (1.6 to 2.9) and the proportion of pyroxenite is low (<5%), this suggests to us that pyroxenite was only a minor component in the mantle sources of the Timbavati sills (Sobolev et al., 2007). Despite the limited mineral compositional data for the Umkondo sills, these findings lend support to the observations made using the Zn/Fe systematics in Fig. 13. More mineral chemical data for the Umkondo sills are needed.

The findings obtained using the Zn/Fe systematics support the assertion that pyroxenite lithologies were part of the sublithospheric mantle source of the Umkondo province, although there appears to be a lack of correlation between Zn/Fe, CaO in olivine, and the PRIMELT3 models. This implies there were varying proportions of peridotite and pyroxenite in the mantle source, with differing degrees of mixing between the melts that were derived from them. The evidence of an enriched mantle component in the Sr-Nd isotopic data (Fig. 8a) may be the same pyroxenite component detected using Zn/Fe as well as in the PRIMELT3 models. Isotopic variability in the mantle sources of OIB suggests that the sublithospheric mantle is heterogeneous and is composed of both peridotite and pyroxenite with the latter originating from recycled oceanic lithosphere (Hofmann, 1997). Another question is whether there was heterogeneous melting of a convecting asthenosphere or a heterogeneous mantle plume. Global studies of radiogenic isotopes in ocean island basalts show that mantle plumes may be heterogeneous in composition (Gibson et al., 2012; Jackson et al., 2012; Weis et al., 2011). Therefore, Umkondo magmatism may have been fed by a heterogeneous mantle plume from the deep Mesoproterozoic mantle.

6.6.3. Did the subcontinental lithospheric mantle contribute?

Some studies have argued that continental flood basalts in southern Africa are derived from the melting of the subcontinental

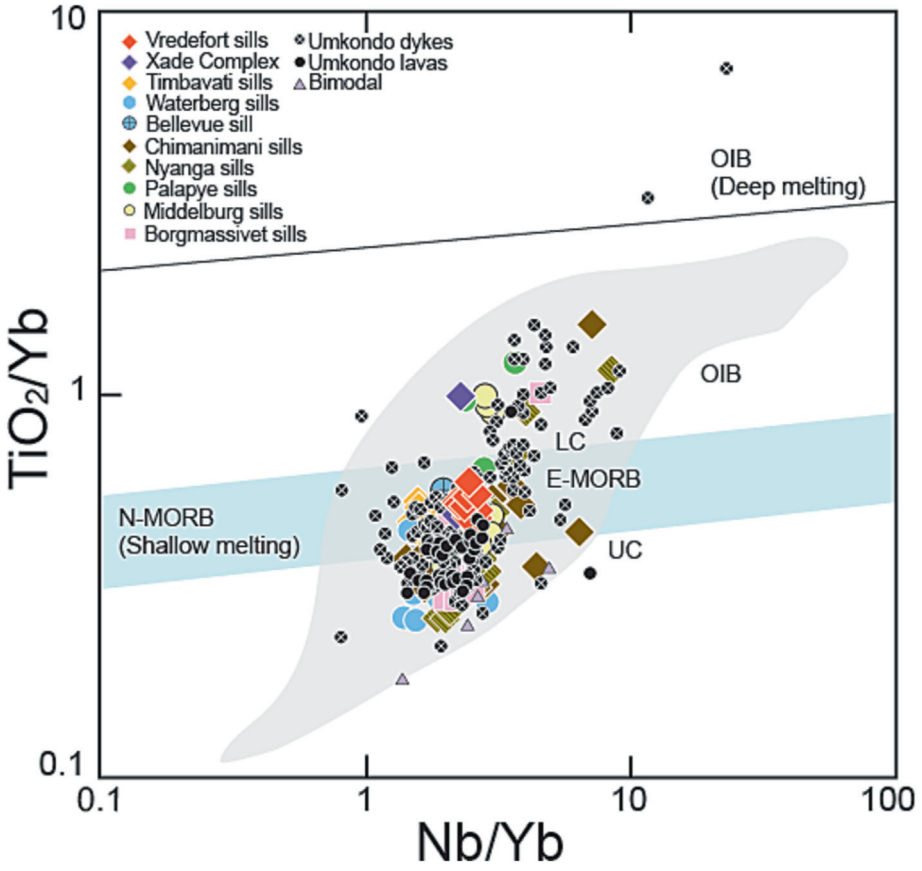


Fig. 12. TiO_2/Yb versus Nb/Yb for the Umkondo province. TiO_2/Yb is a proxy for melting depth and Nb/Yb is a proxy for the melting % and source composition. The fields for N-MORB and OIB are shown. The Karoo province (grey field) is shown for comparison.

lithospheric mantle (e.g., Marsh et al., 1992; Jourdan et al., 2007; Jourdan et al., 2009; de Kock et al., 2014). As we explained above, we consider the sublithospheric mantle to be the major melt contributor to the Umkondo province, although it is probable that the subcontinental lithospheric mantle may have contributed some trace elemental and isotopic signatures via contamination of the ascending magmas. This could happen either by the lithospheric mantle being melted by hot ascending sublithospheric mantle-derived magmas or by the direct melting of the lithospheric mantle and the incorporation of these melts into the sublithospheric mantle-derived magmas. Distinguishing between these two options is, however, problematic (Pearce et al., 2021). There are minor high-Ti and high Ce/Yb alkaline magmas preserved in the Karoo province and are interpreted as direct melts of the subcontinental lithospheric mantle (Ashwal, 2021). These may be the most useful characteristics which can be used to distinguish the presence of melts that are directly derived from the subcontinental lithospheric mantle.

Niobium is sensitive to magma source composition and the role of lithospheric contamination (Fitton et al., 1997; Luttinen, 2018). It has been proposed that the ubiquitous negative Nb anomalies in continental flood basalts are the result of sublithospheric mantle melts acquiring their 'lithospheric signatures' by partial reaction and chemical exchange with lithospheric mantle wall rock (Arndt and Christensen, 1992). The Umkondo province has mostly negative ΔNb (Fig. 10a) and there is a positive correlation between ΔNb and La/Nb (Fig. 10b) and Th/Nb (not shown here) that is consistent with either lithospheric mantle or crustal contamination. The interaction between plume-derived melts and the lithosphere is further supported using the Th/Nb-TiO_2/Yb diagram (Fig. 14) of Pearce et al. (2021). They identified three main arrays using the diagram, with the Type-III array representing the interaction between asthenospheric melts (either MORB or OIB sources) and the subcontinental lithospheric mantle. The Umkondo province forms an array that is comparable to the Type-III array of Pearce et al. (2021) with both OIB and OPB sources evident (Fig. 14). This is similar to other large igneous provinces including Franklin, Columbia River Basalts, Keweenawan and Deccan (Pearce, 2008). However, it is difficult to distinguish this from an array where there was an interaction between asthenospheric melts and continental crust. It is also notable that two groups (high Th/Nb and low Th/Nb) are evident in the Umkondo dykes (Fig. 14).

The Waterberg sills were postulated to represent partial melts of a spinel lherzolite source with its magmas incorporating material from the subduction-modified lithospheric mantle, as interpreted from Sr-Nd isotopes and trace elements (Bullen et al., 2012). A similar petrogenesis was proposed for the Borgmassivet sills with the argument based on (i) the lack of geochemical variation and (ii) the lack of significant correlation between MgO and $^{87}Sr/^{86}Sr$, indicating that the magmas were mostly derived from a sublithospheric mantle source with some amount of crustal and/or lithospheric mantle contamination during transit to the shallow crust (Riley and Millar, 2014). Our Sr-Nd isotopic data for the Vredefort and Timbavati sills, as well as some of the Waterberg sills, are very similar to the Borgmassivet sills, which suggests to us that they have a very similar petrogenetic history. Further isotopic work using less conventional isotopic systems may be required to constrain the role of the subcontinental lithospheric mantle in the evolution of the Umkondo province.

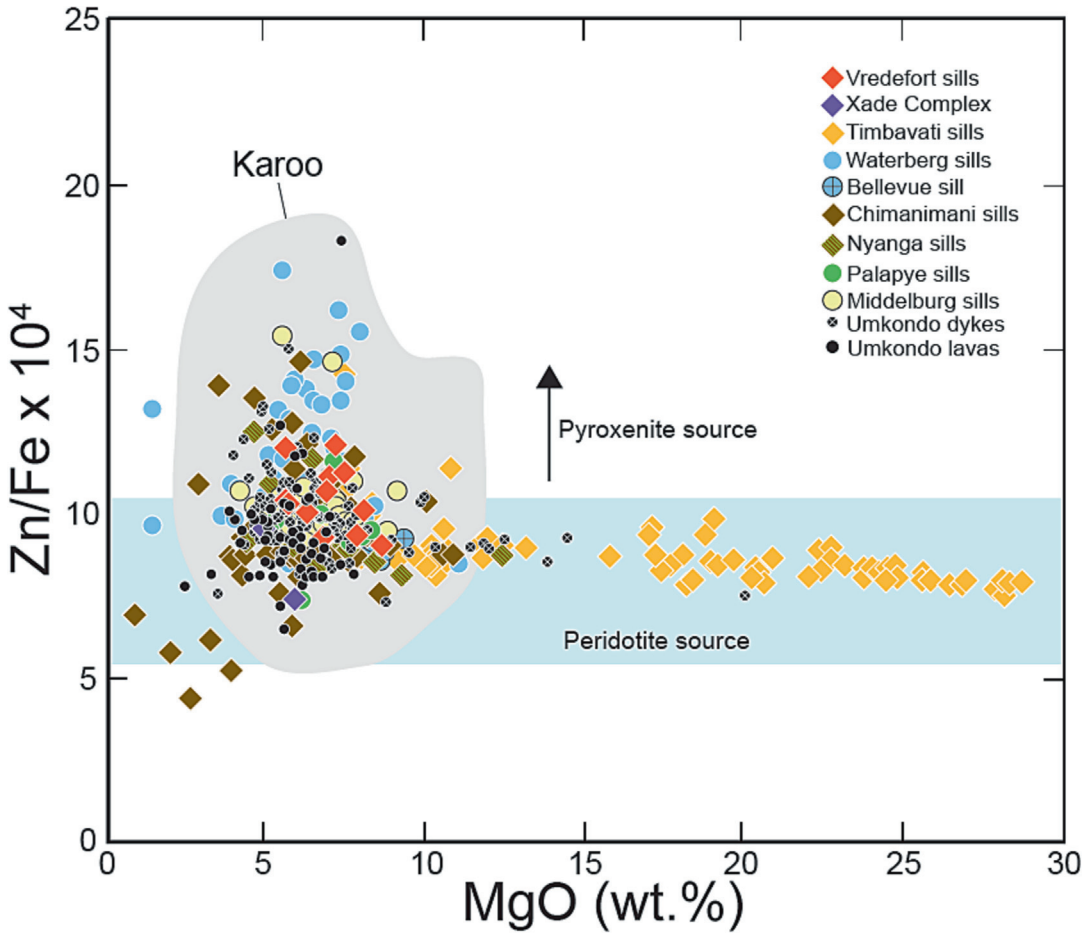


Fig. 13. Zn/Fe ($\times 10^4$) versus MgO (wt.%) for the Umkondo province including fields for a peridotite source and a pyroxenite source (after Le Roux et al., 2010). The Karoo province (grey field) is included for comparison.

6.7. Geochemical linkages between the Umkondo sills and its associated dyke swarms

Many continental flood basalt provinces have radiating dyke swarms associated with them, which may form part of their magmatic plumbing system (e.g., Ernst et al., 1995), and their geochemistry can therefore be used to assess mantle sources in these provinces (e.g., Condie, 1997). There are dyke swarms across southern Africa that have been linked to the Umkondo province and we included them in our geochemical diagrams in this article. Radiating dyke swarms including the Proterozoic Okavango Dyke Swarm, Save-Limpopo Dyke Swarm, Guruve, Kamativi, Mutare and Dibete dykes, appear to converge in central Botswana, near the Xade Complex (Fig. 1). This has been used to infer the 'magmatic centre' of the Umkondo province (de Kock et al., 2014) or may be regarded as the mantle plume impingement site (Ashwal, 2021). The chemistry of the dyke swarms was also used to infer the derivation of Umkondo magmas from subcontinental lithospheric mantle sources (de Kock et al., 2014). The Umkondo dykes may therefore provide important insights into the origin of the Umkondo province and its tectonic setting.

All the chemical variation diagrams presented in this article suggest that the Umkondo dykes show the widest compositional ranges. Some of the most depleted and enriched isotope values are preserved in the dykes (initial $^{87}Sr/^{86}Sr$ ranges from 0.703008 to 0.757554 and εNd ranges from 7.4 to −15.6; Fig. 8a). Some of the most isotopically depleted dyke compositions are comparable to the Vredefort sills (Fig. 8a). The Mutare dykes have εNd of 7.3 to −7.8, with the Kamativi dykes having εNd of 4.3 to −3.6, and the Guruve dykes have εNd of 1 to −15 (Fig. 8a). The dykes that have depleted mantle-like sources are also part of the high-Ti and high Ce/Yb magma suite which is only rarely recognised in the Umkondo sills. These dykes also have some of the highest Sm/Yb and may be derived from deep garnet-bearing mantle sources (Arndt et al., 1998). Two chemical groups of dykes are evident in Fig. 14, one with high Th/Nb and one with low Th/Nb. The low Th/Nb group also have some of the highest Sm/Yb. These findings may be significant as the dykes record considerable heterogeneity in the Umkondo province, and they may record the whole range of chemical end members involved in the petrogenesis of the Umkondo province. However, we urge caution in making such claims until more age constraints are obtained for the dykes that conclusively show they are all part of the Umkondo province.

6.8. Implications for the assembly and configuration of Rodinia at 1.11 Ga during the 'boring billion'

The timing of Umkondo magmatism broadly coincides with the assembly of the Rodinia supercontinent (e.g., Meert and Torsvik, 2003). In most traditional continent configurations of Rodinia, the Kalahari craton is separated from Laurentia (Dalziel, 2023), however, its precise position remains poorly constrained (Meert and Torsvik, 2003). The Kalahari craton is also thought to be situated adjacent to the Grunehogna terrane of Dronning Laud Land at ca. 1.11 Ga (Dalziel, 2023) as shown in Fig. 1. The similar U-Pb ages and Sr-Nd isotopic signatures of the Borgmassivet sills with

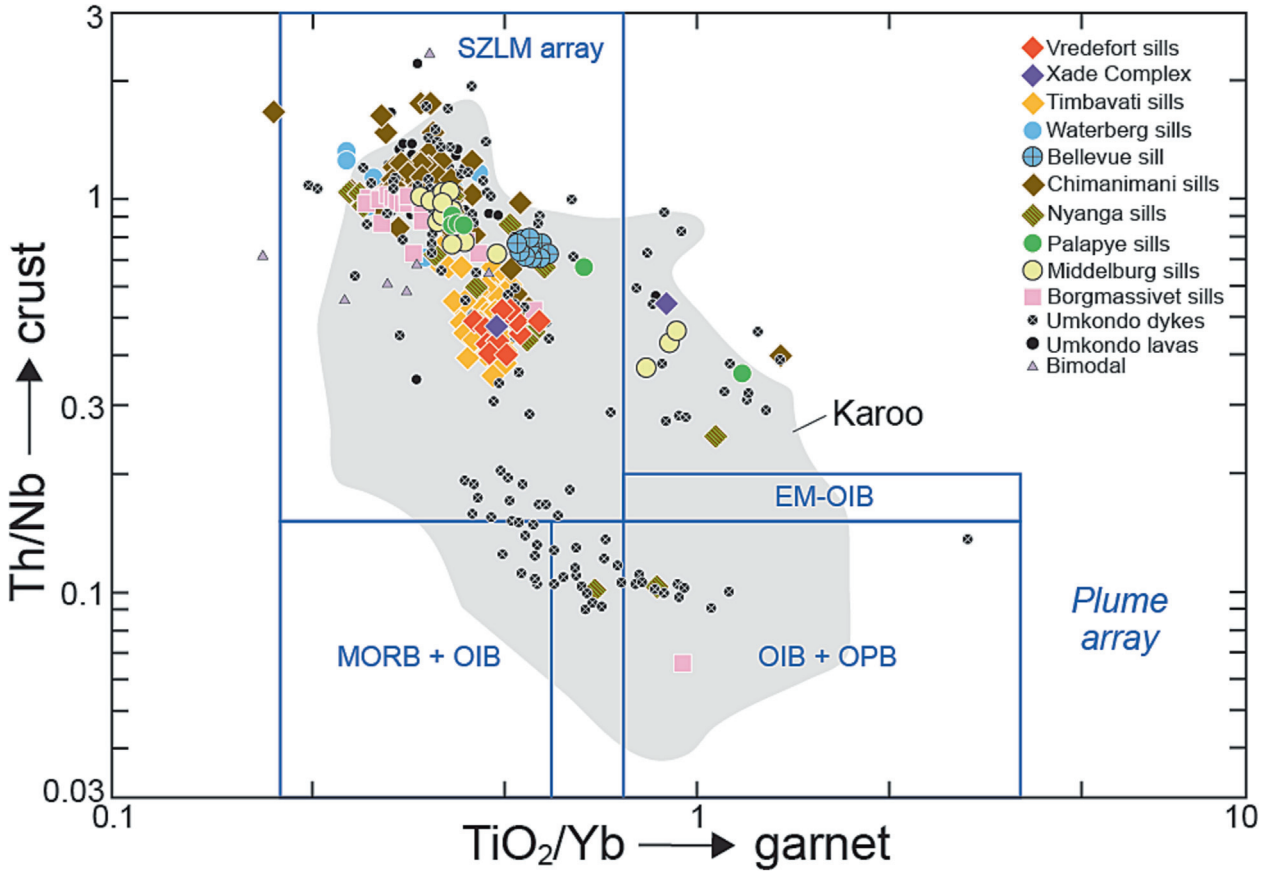


Fig. 14. Th/Nb (crustal input) versus TiO_2/Yb (garnet in the source) with various mantle sources defined (Pearce et al., 2021). The Umkondo province mostly plots in the SZLM field (i.e., subcontinental lithospheric mantle) and forms a trend that is comparable to Type-IIIb that suggests the interaction of SZLM and OIB (Pearce et al., 2021).

the Vredefort, Timbavati and Waterberg sills (Fig. 8a) lend support to a connection between the Kalahari craton and Grunehogna terrane at 1.11 Ga.

The timing of Umkondo magmatism at the onset of Rodinia is at odds with the typical notion of continental flood basalt magmatism being related to periods of crustal extension and continental breakup (e.g., Courtillot et al., 1999) although it has been shown that the emplacement of large igneous provinces does not necessarily correspond with large-scale continental breakup events in the geological record (e.g., Ernst, 2014). It has also been recently proposed that the tectonic regime during the 'boring billion' was dominated by accordion-style tectonics with episodes of extension, continental breakup, and asthenospheric mantle upwelling followed by episodes of compression and basin closure (Santosh and Groves, 2023). The Umkondo province may represent an episode of extensional tectonics, possibly in a back-arc (e.g., Klausen, 2020), during the assembly of Rodinia with a mantle plume that induced large-scale melting of the sublithospheric mantle beneath this portion of the Kalahari craton.

Some authors have correlated the Umkondo province to the earliest phase of basaltic magmatism of the Midcontinent rift on Laurentia (Hanson et al., 2004; Swanson-Hysell et al., 2015). However, parts of the Midcontinent rift are significantly younger (ca. 20 Myr) than the Umkondo province (Hanson et al., 2004; Vervoort et al., 2007), so the possible genetic relations between the two provinces remain to be tested in more detail. Furthermore, the Ni-Cu-PGE mineralised Duluth Complex is part of the Midcontinent Rift. In the Umkondo province, the association of continental breakup, plume-driven magmatism generating komatiitic magmas, and the geochemical evidence of crustal assimilation, raise the prospect of magmatic Ni-Cu-PGE sulphide ore deposits related to this province. A good candidate for hosting these types of ore deposits is the Xade Complex, which has been previously explored for Ni-Cu-PGE mineralisation.

7. Conclusions

The Mesoproterozoic (1.11 Ga) Umkondo large igneous province is distributed across southern Africa and Antarctica and is mostly preserved as dolerite-gabbro sills that were emplaced into Archean granite-gneisses and Paleoproterozoic sedimentary successions. The Umkondo province has been poorly studied and there are few constraints on the nature of its magma sources and the compositional evolution of its magmas. In this study, we compiled existing and new major and trace element data, supplemented with 42 new Sr-Nd isotope measurements, to unravel the magmatic evolution of the Umkondo province. The sills have major and trace element chemical signatures typical of continental flood basalt provinces that are sub-alkaline basalt to basaltic-andesites, and which are mostly low-Ti (<1.5 wt.% TiO_2) with enrichment in incompatible trace elements and light/heavy rare earth elements (Ce/Yb $\geq$ 10). The major element compositions show that the Umkondo magmas are residual liquids (~10 wt.% MgO) of primary magmas that underwent three-phase (olivine-pyroxene-plagioclase) fractional crystallization. Inverse models in PRIMELT3 show that the primary magmas were komatiites (up to 20 wt.% MgO). Sm/Yb is low (<2) and indicative of the primary magmas being derived by shallow melting of spinel lherzolite. The enrichment in light/heavy rare earth elements and evolved initial Sr-Nd isotopic compositions show that the Umkondo magmas

incorporated significant quantities of crustal and/or lithospheric material. This is supported by various trace element proxies, although it is challenging to distinguish between these two enriched reservoirs. The mantle source of the Umkondo magmas was mainly the sublithospheric mantle as shown by the high MgO and high temperatures of its primary magmas as well as the large volume and short duration of Umkondo magmatism. The sublithospheric mantle source was heterogeneous with both peridotite and pyroxenite lithologies. The Vredefort and Borgmassivet sills are the least contaminated and appear to represent near-primary magma compositions for the Umkondo province. The timing of Umkondo magmatism suggests that there was local extension and plume upwelling on the Kalahari craton at the earliest stages of Rodinia assembly.

Declaration of Competing Interest

The authors declare that they have no known competing financial interests or personal relationships that could have appeared to influence the work reported in this paper.

Acknowledgements

We extend our gratitude to Dean Bullen and Richard Hanson for generously providing some of our Umkondo samples for further trace element and isotopic analyses. Rais Latypov provided the major and trace element data for the Bellevue sill. We are indebted to Tony Martin for field support in eastern Zimbabwe in 2019. Marlin Patchappa performed the XRF and ICP-MS analyses in the Earth Laboratory at Wits. Henriette Ueckermann greatly assisted with the isotopic measurements at the University of Johannesburg. Caiphas Majola, Sam Tshabalala, and Louis Mudalahothe provided the thin sections. A generous grant from the Oppenheimer Memorial Trust (21052/01) as well as financial and logistical support from DSI-NRF CIMERA supported this research. This manuscript greatly benefited from the comments of three anonymous reviewers.

Appendix A. Supplementary data

Supplementary data to this article can be found online at https://doi.org/10.1016/j.gsf.2023.101719.

References

Allsopp, H.J., Kramers, J.D., Jones, D.L., Erlank, A.J., 1989. The age of the Umkondo Group, Eastern Zimbabwe, and implications for palaeomagnetic correlations. S. Afr. J. Geol. 92 (1), 11–19.
Andersen, D.L., 1994. The sublithospheric mantle as the source of continental flood basalts; The case against the continental lithosphere and plume head reservoirs. Earth Planet. Sci. Lett. 123 (1), 269–280.
Arndt, N.T., Christensen, U., 1992. The role of lithospheric mantle in continental flood volcanism; Thermal and geochemical constraints. J. Geophys. Res.: Solid. Earth 97, 10967–10981.
Arndt, N.T., Czamanske, G.K., Wooden, J.L., Fedorenko, V.A., 1993. Mantle and crustal contributions to continental flood volcanism. Tectonophysics 223 (1–2), 39–52.
Arndt, N.T., Chauvel, C., Czamanske, G.K., Fedorenko, V., 1998. Two mantle sources, two plumbing systems: Tholeiitic and alkaline magmatism of the Maymecha River Basin, Siberian flood volcanic province. Contrib. Miner. Petrol. 133 (3), 297–313.
Ashwal, L.D., 2021. Sub-lithospheric mantle sources for overlapping southern African large igneous provinces. S. Afr. J. Geol. 124 (2), 421–442.
Ashwal, L.D., Ziegler, A., Glynn, S., Truebody, T., Bolhar, R., 2021. Sr-enriched glassy picrites from the Karoo large igneous province are evolved, not primitive magmatic rocks. Geochem. Geophys. Geosyst. 22, e2020GC009561. https://doi.org/10.1029/2020GC009561.
Ashwal, L.D., Webb, S.J., Knoper, M.W., 2005. Magmatic stratigraphy in the Bushveld Northern Lobe; Continuous geophysical and mineralogical data from the 2950 m Bellevue drillcore. S. Afr. J. Geol. 108 (2), 199–232.
Beard, C.D., Scoates, J.S., Weis, D., Bédard, J.H., Dell'Oro, T.A., 2017. Geochemistry and origin of the Neoproterozoic Natkusiak flood basalts and related Franklin sills, Victoria Island. Arctic Canada. J. Petrol. 58 (11), 2191–2220.
Bédard, J.H., Saumur, B.M., Tegner, C., Troll, V.R., Deegan, F.M., Evenchick, C.A., Grasby, S.E., Dewing, K., 2021. Geochemical systematics of High Arctic large igneous province continental tholeiites from Canada-Evidence for progressive crustal contamination in the plumbing system. J. Petrol. 62 (9), egab041. https://doi.org/10.1093/petrology/egab041.
Bourdeau, J.E., Hayes, B., Zhang, S.E., Logue, A., Bybee, G.M., 2022. Origin and significance of noritic blocks in layered anorthosites in the Bushveld Complex, South Africa. Contrib. Mineral. Petrol. 177 (1), 1–26.
Bristow, J.W., Armstrong, R.A., Allsopp, H.L., 1982. A note on the geology and geochronology of the Tsange gabbros. Trans. Geol. Soc. S. Afr. 85 (3), 135–139.
Bullen, D.S., 2005. The petrology of Proterozoic mafic sills in southern Africa. PhD thesis. University of Portsmouth, p. 397.
Bullen, D.S., Hall, R.P., Hanson, R.E., 2012. Geochemistry and petrogenesis of mafic sills in the 1.1 Ga Umkondo large igneous province, southern Africa. Lithos 142, 116–129.
Carlson, R.W., Lugmair, G.W., Macdougall, J.D., 1981. Columbia River volcanism; The question of mantle heterogeneity of crustal contamination. Geochim. Cosmochim. Acta 45 (12), 2483–2499.
Choudhary, B.R., Ernst, R.E., Xu, G.Y., Evans, D.A.D., de Kock, M.O., Meert, J.G., Ruiz, A. S., Lima, G.A., 2019. Geochemical characterization of a reconstructed 1110 Ma large igneous province. Precambr. Res. 332,. https://doi.org/10.1016/j.precamres.2019.105382 105382.
Cole, J., Finn, C.A., Webb, S.J., 2021. Geometry of the Bushveld Complex from 3D potential field modelling. Precambr. Res. 359, 106219.
Coltice, N., Bertrand, H., Rey, P., Jourdan, F., Phillips, B.R., Ricard, Y., 2009. Global warming of the mantle beneath continents back to the Archaean. Gondw. Res. 15 (3–4), 254–266.
Condie, K.C., 1997. Sources of Proterozoic mafic dyke swarms; Constraints from Th-Ta and La-Yb ratios. Precambr. Res. 81 (1–2), 3–14.
Condie, K.C., 2001. Mantle Plumes and Their Record in Earth History. Cambridge University Press, p. 306.
Corner, B., Verran, D.R., Hildebrand, P.R., 2012. Geophysical interpretation of the nature and extent of the Xade Mafic Complex, Botswana. S. Afr. J. Geol. 115 (4), 485–498.
Courtillot, V., Jaupart, C., Manighetti, I., Tapponnier, P., Besse, J., 1999. On casual links between flood basalts and continental breakup. Earth Planet. Sci. Lett. 166 (3–4), 177–195.
Courtillot, V.E., Renne, P.R., 2003. On the ages of flood basalt events. C. R. Geosci. 335 (1), 113–140.
Cox, K.G., 1980. A model for flood basalt volcanism. J. Petrol. 21 (4), 629–650.
Cox, K.G., MacDonald, R., Hornung, G., 1967. Geochemical and petrographic provinces in the Karroo basalts of southern Africa. Am. Mineral. 52 (9–10), 1451–1474.
Dalziel, I.W., 2023. Rodinia palaeogeography: Laurentia as the geological 'Key'. Geol. Soc. London Spec. Pub. 542 (1), SP542-2022.
de Kock, M.O., Ernst, R.E., Söderlund, U., Jourdan, F., Hofmann, A., Le Gall, B., Bertrand, H., Chisonga, B.C., Beukes, N., Rajesh, H.M., 2014. Dykes of the 1.11 Ga Umkondo LIP, southern Africa; Clues to a complex plumbing system. Precambr. Res. 249, 129–143.
DePaolo, D.J., 1981. Trace element and isotopic effects of combined wallrock assimilation and fractional crystallization. Earth Planet. Sci. Lett. 53 (2), 189–202.
Dockman, D.M., Pearson, D.G., Heaman, L.M., Gibson, S.A., Sarkar, C., 2018. Timing and origin of magmatism in the Sverdrup Basin, northern Canada-Implications for lithospheric evolution in the High Arctic large igneous province (HALIP). Tectonophysics 742, 50–65.
Elburg, M., Goldberg, A., 2000. Age and geochemistry of Karoo dolerite dykes from northeast Botswana. J. Afr. Earth Sci. 31 (3–4), 539–554.
Ellam, R.M., Cox, K.G., 1991. An interpretation of Karoo picrite basalts in terms of interaction between asthenospheric magmas and the mantle lithosphere. Earth Planet. Sci. Lett. 105 (1–3), 330–342.
Ernst, R.E., 2014. Large Igneous Provinces. Cambridge University Press, p. 653.
Ernst, R.E., Head, J.W., Parfitt, E., Grosfils, E., Wilson, L., 1995. Giant radiating dyke swarms on Earth and Venus. Earth Sci. Rev. 39 (1–2), 1–58.
Ernst, R.E., Pereira, E., Hamilton, M.A., Pisarevsky, S.A., Rodriques, J., Tassinari, C.G., Teixeira, W., Van-Dunem, V., 2013. Mesoproterozoic intraplate magmatic 'barcode' record of the Angola portion of the Congo Craton; Newly dated magmatic events at 1505 and 1110 Ma and implications for Nuna (Columbia) supercontinent reconstructions. Precambr. Res. 230, 103–118.
Fitton, J.G., Saunders, A.D., Norry, M.J., Hardarson, B.S., Taylor, R.N., 1997. Thermal and chemical structure of the Iceland plume. Earth Planet. Sci. Lett. 153 (3–4), 197–208.
Gallagher, K., Hawkesworth, C., 1992. Dehydration melting and generation of continental flood basalts. Nature 358 (6381), 57–59.
Ghiorso, M.S., Gualda, G.A., 2015. An H_2O-CO_2 mixed fluid saturation model compatible with rhyolite-MELTS. Contrib. Miner. Petrol. 169 (6), 1–30.
Gibson, S.A., Geist, D.G., Day, J.A., Dale, C.W., 2012. Short wavelength heterogeneity in the Galapagos plume: Evidence from compositionally diverse basalts on Isla Santiago. Geochem. Geophys. Geosyst. 13 (9), Q09007.
Gose, W.A., Hanson, R.E., Dalziel, I.W.D., Pancake, J.A., Seidel, E.K., 2006. Paleomagnetism of the 1.1 Ga Umkondo large igneous province in southern Africa. J. Geophys. Res.: Solid Earth 111, B09101. https://doi.org/10.1029/2005JB003897.
Groenewald, P.B., Moyes, A.B., Grantham, G.H., Krynauw, J.R., 1995. East Antarctic crustal evolution; Geological constraints and modelling in western Dronning Maud Land. Precambr. Res. 75 (3–4), 231–250.

Gualda, G.A., Ghiorso, M.S., Lemons, R.V., Carley, T.L., 2012. Rhyolite-MELTS: A modified calibration of MELTS optimized for silica-rich, fluid-bearing magmatic systems. J. Petrol. 53 (5), 875–890.
Hanson, R.E., Martin, M.W., Bowring, S.A., Munyanyiwa, H., 1998. U-Pb zircon age for the Umkondo dolerites, eastern Zimbabwe; 1.1 Ga large igneous province in southern Africa-east Antarctica and possible Rodinia correlations. Geology 26 (12), 1143–1146.
Hanson, R.E., Crowley, J.L., Bowring, S.A., Ramezani, J., Gose, W.A., Dalziel, I.W.D., Pancake, J.A., Seidel, E.K., Blenkinsop, T.G., Mukwakwami, J., 2004. Coeval large-scale magmatism in the Kalahari and Laurentian cratons during Rodinia assembly. Science 304 (5674), 1126–1129.
Hanson, R.E., Harmer, R.E., Blenkinsop, T.G., Bullen, D.S., Dalziel, I.W.D., Gose, W.A., Hall, R.P., Kampunzu, A.B., Key, R.M., Mukwakwami, J., 2006. Mesoproterozoic intraplate magmatism in the Kalahari craton. A review. J. Afr. Earth Sci. 46 (1–2), 141–167.
Hargraves, R.N., 1994. Palaeomagnetic results from the Timbavati gabbros in the Kruger National Park, South Africa. S. Afr. J. Geol. 97 (2), 114–118.
Hart, S.R., Hauri, E.H., Oschmann, L.A., Whitehead, J.A., 1992. Mantle plumes and entrainment. Isotopic evidence. Science 256 (5056), 517–520.
Heinonen, J.S., Luttinen, A.V., Riley, T.R., Michallik, R.M., 2013. Mixed pyroxenite-peridotite sources for mafic and ultramafic dikes from the Antarctic segment of the Karoo continental flood basalt province. Lithos 177, 366–380.
Heinonen, J.S., Luttinen, A.V., Bohrson, W.A., 2016. Enriched continental flood basalts from depleted mantle melts; Modeling the lithospheric contamination of Karoo lavas from Antarctica. Contrib. Miner. Petrol. 171 (1), 1–22.
Herzberg, C., Asimow, P.D., 2015. PRIMELT3 MEGA.XLSM software for primary magma calculation; peridotite primary magma MgO contents from the liquidus to the solidus. Geochem. Geophys. Geosyst. 16 (2), 563–578.
Hofmann, A.W., 1997. Mantle geochemistry; The message from oceanic volcanism. Nature 385 (6613), 219–229.
Howarth, G.H., Harris, C., 2017. Discriminating between pyroxenite and peridotite sources for continental flood basalts (CFB) in southern Africa using olivine chemistry. Earth Planet. Sci. Lett. 475, 143–151.
Jackson, M.G., Weis, D., Huang, S., 2012. Major element variations in Hawaiian shield lavas: Source features and perspectives from global ocean island basalt (OIB) systematics. Geochem. Geophys. Geosyst. 13 (9), Q09009.
Jones, D.L., Bates, M.P., Li, Z.-X., Corner, B., Hodgkinson, G., 2003. Palaeomagnetic results from the ca. 1130 Ma Borgmassivet intrusions in the Ahlmannryggen region of Dronning Maud Land, Antarctica, and tectonic implications. Tectonophysics 375 (104), 247–260.
Jones, D.L., McElhinny, M.W., 1966. Paleomagnetic correlation of basic intrusions in the Precambrian of southern Africa. J. Geophys. Res. 71 (2), 543–552.
Jourdan, F., Bertrand, H., Schärer, U., Blichert-Toft, J., Féraud, G., Kampunzu, A.B., 2007. Major and trace element and Sr, Nd, Hf, and Pb isotope compositions of the Karoo large igneous province, Botswana-Zimbabwe; Lithospheric vs mantle plume contribution. J. Petrol. 48 (6), 1043–1077.
Jourdan, F., Bertrand, H., Féraud, G., Le Gall, B., Watkeys, M.K., 2009. Lithospheric mantle evolution monitored by overlapping large igneous provinces; A case study in southern Africa. Lithos 107 (3–4), 257–268.
Klausen, M.B., 2020. Conditioned duality between supercontinental 'assembly' and 'breakup' LIPs. Geosci. Front., 1635–1649
Le Maitre, R.W., 1984. A proposal by the IUGS Subcommission on the systematics of igneous rocks for a chemical classification of volcanic rocks based on the total alkali-silica (TAS diagram); on behalf of the IUGS Subcommission of igneous rocks. Aust. J. Earth Sci. 31 (2), 243–255.
Le Roux, V., Lee, C.-T.-A., Turner, S.J., 2010. Zn/Fe systematics in mafic and ultramafic systems; Implications for detecting major element heterogeneities in the Earth's mantle. Geochim. Cosmochim. Acta 74 (9), 2779–2796.
Luttinen, A.V., 2018. Bilateral geochemical asymmetry in the Karoo large igneous province. Sci. Rep. 8 (1), 1–11.
Marsh, J.S., Bowen, M.P., Rogers, N.W., Bowen, T.B., 1992. Petrogenesis of late Archaean flood-type basic lavas from the Klipriviersberg Group, Ventersdorp Supergroup. South Africa. J. Petrol. 33 (4), 817–847.
Matzen, A.K., Baker, M.B., Beckett, J.R., Stolper, E.M., 2011. Fe-Mg partitioning between olivine and high-magnesian melts and the nature of Hawaiian parental liquids. J. Petrol. 52 (7–8), 1243–1263.
McDonough, W.F., Sun, S.-S., 1995. The composition of the Earth. Chem. Geol. 120 (3–4), 223–253.
McElhinny, M.W., Opdyke, N.D., 1964. The Palaeomagnetism of the Precambrian dolerites of eastern southern Rhodesia, an example of geologic correlation by rock magnetism. J. Geophys. Res. 69 (12), 2465–2475.
Meert, J.G., Torsvik, T.H., 2003. The making and unmaking of a supercontinent: Rodinia revisited. Tectonophysics 375 (1–4), 261–288.
Moabi, N.G., Grantham, G.H., Roberts, J., Le Roux, P., Matola, R., 2015. The geology and geochemistry of the Espungabera Formation of central Mozambique and its tectonic setting on the eastern margin of the Kalahari craton. J. Afr. Earth Sc. 101, 96–112.
Moabi, N.G., Grantham, G.H., Roberts, J., Le Roux, P., 2017. The geology and geochemistry of the Straumsnutane Formation, Straumsnutane, western Dronning Maud Land, Antarctica and its tectonic setting on the western margin of the Kalahari craton; Additional evidence linking it to the Umkondo large igneous province. Geol. Soc. London Spec. Pub. 457 (1), 61–85.
Moyes, A.B., Krynauw, J.R., Barton, J.M., 1995. The age of the Ritscherflya Supergroup and Borgmassivet intrusions, Dronning Maud Land, Antarctica. Antarct. Sci. 7 (1), 87–97.
Muedi, T.S., MacLennan, S.A., Szymanowski, D., Schoene, B., Ramezani, J., Oalmann, J., Linol, B., 2022. Constraining the timescales of mafic magmatism of the central Karoo large igneous province using high precision U-Pb zircon geochronology. S. Afr. J. Geol. 125 (1), 99–112.
Munyanyiwa, H., 1999. Geochemical study of the Umkondo dolerites and lavas in the Chimanimani and Chipinge districts (eastern Zimbabwe) and their regional implications. J. Afr. Earth Sc. 28 (2), 349–365.
Pancake, J.A., 2001. Palaeomagnetism and geochronology of Mesoproterozoic mafic and felsic sills in southeast Botswana. MS thesis. Texan Christian University, p. 163.
Pearce, J.A., 2008. Geochemical fingerprinting of oceanic basalts with applications to ophiolite classification and the search for Archean oceanic crust. Lithos 100 (1–4), 14–48.
Pearce, J.A., Ernst, R.E., Peate, D.W., Rogers, C., 2021. LIP printing: Use of immobile element proxies to characterise large igneous provinces in the geologic record. Lithos 392,. https://doi.org/10.1016/j.lithos.2021.106068 106068.
Reimold, W.U., Pybus, G.Q.J., Kruger, F.J., Layer, P.W., Koeberl, C., 2000. The Anna's Rust Sheet and related gabbroic intrusions in the Vredefort Dome-Kibaran magmatic event on the Kaapvaal craton and beyond? J. Afr. Earth Sc. 31 (3–4), 499–521.
Riley, T.R., Millar, I.L., 2014. Geochemistry of the 1100 Ma intrusive rocks from the Ahlmannryggen region, Dronning Maud Land, Antarctica. Antarct. Sci. 26 (4), 389–399.
Rooney, T.O., Nelson, W.R., Ayalew, D., Hanan, B., Yirgu, G., Kappelman, J., 2017. Melting the lithosphere: Metasomes as a source for mantle-derived magmas. Earth Planet. Sci. Lett. 461, 105–118.
Salminen, J., Hanson, R.E., Evans, D.A.D., Gong, Z., Larson, T., Walker, O., Gumsley, A., Söderlund, U., Ernst, R.E., 2018. Direct Mesoproterozoic connection of the Congo and Kalahari cratons in proto-Africa. Strange attractors across Supercontinental cycles. Geology 46 (11), 1011–1014.
Santosh, M., Groves, D.I., 2023. The Not-So-Boring Billion: A metallogenetic conundrum during the evolution from Columbia to Rodinia supercontinents. Earth Sci. Rev. 104287.
Saunders, A.D., Norry, M.J., Tarney, J., 1988. Origin of MORB and chemically-depleted mantle reservoirs; Trace element constraints. J. Petrol. 1, 415–445.
Shellnutt, J.G., 2014. The Emeishan large igneous province: a synthesis. Geosci. Front. 5 (3), 369–394.
Sobolev, A.V., Hofmann, A.W., Kuzmin, D.V., Yaxley, G.M., Arndt, N.T., Chung, S.-L., Danyushevsky, L.V., Elliott, T., Frey, F.A., Garcia, M.O., 2007. The amount of recycled crust in sources of mantle-derived melts. Science 316 (5823), 412–417.
Sun, S.-S., McDonough, W.F., 1989. Chemical and isotopic systematics of oceanic basalts; Implications for mantle composition and processes. Geol. Soc. London Spec. Pub. 42 (1), 313–345.
Svensen, H., Corfu, F., Polteau, S., Hammer, Ø., Planke, S., 2012. Rapid magma emplacement in the Karoo large igneous province. Earth Planet. Sci. Lett. 325, 1–9.
Swanson-Hysell, N.L., Kilian, T.M., Hanson, R.E., 2015. A new grand mean palaeomagnetic pole for the 1.11 Ga Umkondo large igneous province with implications for palaeogeography and the geomagnetic field. Geophysical Supplements to the Monthly Notices of the Royal Astronomical Society 203 (3), 2237–2247.
Tegner, C., Michelis, S.A.T., McDonald, I.D., Brown, E.L., Youbi, N., Callegaro, S., Lindström, S., Marzoli, A., 2019. Mantle dynamics of the Central Atlantic Magmatic Province (CAMP); Constraints from Platinum Group, Gold and Lithophile elements in flood basalts of Morocco. J. Petrol. 60 (8), 1621–1652.
Turner, S.J., Hawkesworth, C., Gallagher, K., Stewart, K., Peate, D., Mantovani, M., 1996. Mantle plumes, flood basalts, and thermal models for melt generation beneath continents; Assessment of a conductive heating model and application to the Paraná. J. Geophys. Res.: Solid Earth 101 (B5), 11503–11518.
Vervoort, J.D., Wirth, K., Kennedy, B., Sandland, T., Harpp, K.S., 2007. The magmatic evolution of the Midcontinent rift: New geochronologic and geochemical evidence from felsic magmatism. Precambr. Res. 157, 235–268.
Ward, S.E., 2002. The petrogenesis of the Mesoproterozoic mafic dykes and sills of Zimbabwe. PhD thesis, University of Portsmouth, 357 pp.
Watson, R.L.A., 1969. The geology of the Cashel, Melsetter and Chipinga areas. Bulletin of the Geological Survey of Rhodesia 60, 85 pp.
Weis, D., Garcia, M.O., Rhodes, J.M., Jellinek, M., Scoates, J.S., 2011. Role of the deep mantle in generating the compositional asymmetry of the Hawaiian mantle plume. Nat. Geosci. 4 (12), 831–838.
White, R.S., McKenzie, D.A., 1995. Mantle plumes and flood basalts. J. Geophys. Res.: Solid Earth 100 (B9), 17543–17585.
Wilson, J.F., Jones, D.L., Kramers, J.D., Halls, H.C., Fahrig, W.F., 1987. Mafic dyke swarms in Zimbabwe. Mafic Dyke Swarms, Geological Association of Canada Special Paper 34, 433–444.
Wooden, J.L., Czamanske, G.K., Fedorenko, V.A., Arndt, N.T., Chauvel, C., Bouse, R.M., King, B.S.W., Knight, R.J., Siems, D.F., 1993. Isotopic and trace-element constraints on the mantle and crustal contributions to Siberian continental flood basalts, Noril'sk area, Siberia. Geochim. Cosmochim. Acta 57 (15), 3677–3704.
Xu, Y.G., He, B., Chung, S.L., Menzies, M.A., Frey, F.A., 2004. Geologic, geochemical, and geophysical consequences of plume involvement in the Emeishan flood-basalt province. Geology 32 (10), 917–920.
Zhang, H.-F., Goldstein, S.L., Zhou, X.-H., Sun, M., Zheng, J.-P., Cai, Y., 2008. Evolution of subcontinental lithospheric mantle beneath eastern China; Re-Os isotopic evidence from mantle xenoliths in Paleozoic kimberlites and Mesozoic basalts. Contrib. Miner. Petrol. 155 (3), 271–293.